

# Recent progress and future prospects of perovskite tandem solar cells

Cite as: Appl. Phys. Rev. **8**, 041307 (2021); doi: [10.1063/5.0061483](https://doi.org/10.1063/5.0061483)

Submitted: 26 June 2021 · Accepted: 31 August 2021 ·

Published Online: 15 October 2021



View Online



Export Citation



CrossMark

Anita W. Y. Ho-Baillie,<sup>1,2,3,a)</sup> Jianghui Zheng,<sup>1,2,3,a)</sup> Md Arafat Mahmud,<sup>1,2</sup> Fa-Jun Ma,<sup>3</sup> David R. McKenzie,<sup>1</sup> and Martin A. Green<sup>3</sup>

## AFFILIATIONS

<sup>1</sup>School of Physics, The University of Sydney, Sydney, New South Wales 2006, Australia

<sup>2</sup>The University of Sydney Nano Institute (Sydney Nano), The University of Sydney, Sydney, New South Wales 2006, Australia

<sup>3</sup>Australian Centre for Advanced Photovoltaics, School of Photovoltaic and Renewable Energy Engineering, University of New South Wales, Sydney 2052, Australia

<sup>a)</sup>Authors to whom correspondence should be addressed: [anita.ho-baillie@sydney.edu.au](mailto:anita.ho-baillie@sydney.edu.au); and [jianghui.zheng@sydney.edu.au](mailto:jianghui.zheng@sydney.edu.au)

## ABSTRACT

Organic-inorganic metal halide perovskite solar cells represent the fastest advancing solar cell technology in terms of energy conversion efficiency improvement, as seen in the last decade. This has become a promising technology for next-generation, low-cost, high-efficiency photovoltaics including multi-junction tandem cell concepts. Double-junction tandem cells have much higher efficiency limits of 45%, beyond the Shockley–Queisser limits for a single-junction solar cell. In this review, recent progress with the perovskite tandem solar cells is highlighted, in particular, with 2-terminal perovskite–Si, perovskite–CIGS [where CIGS = Cu(In,Ga)(S,Se)<sub>2</sub>], perovskite–organic photovoltaic, perovskite–perovskite, and 3-junction-perovskite tandems. The opportunity and challenges of two-terminal monolithic perovskite tandems are discussed including a roadmap of strategies for further improving their efficiencies.

© 2021 Author(s). All article content, except where otherwise noted, is licensed under a Creative Commons Attribution (CC BY) license (<http://creativecommons.org/licenses/by/4.0/>). <https://doi.org/10.1063/5.0061483>

## TABLE OF CONTENTS

I. OVERVIEW OF TANDEM SOLAR CELLS AND OPPORTUNITIES FOR TANDEM SOLAR CELLS USING PEROVSKITES .....	1
II. RECENT PROGRESS OF TANDEM SOLAR CELLS USING PEROVSKITES .....	3
A. Perovskite–silicon tandem solar cells.....	4
B. Perovskite–CIGS tandem solar cells.....	10
C. Perovskite–OPV tandem solar cells.....	14
D. Perovskite–perovskite tandem solar cells .....	14
E. Triple-junction .....	19
F. Future prospects for perovskite tandem solar cells .....	20
III. CONCLUSION AND OUTLOOK .....	21
AUTHORS' CONTRIBUTIONS.....	21
<b>I. OVERVIEW OF TANDEM SOLAR CELLS AND OPPORTUNITIES FOR TANDEM SOLAR CELLS USING PEROVSKITES</b>	

Crystalline silicon based solar cell technology currently dominates the commercial photovoltaic market due to its robustness in

terms of manufacturing technology, product reliability, and low manufacturing costs, which have dropped significantly in the last decade fueling the exponential growth in global installations.<sup>1,2</sup> However, the incumbent technology is based on a single-junction silicon solar cell, which inherently is limited in terms of power conversion efficiency (PCE). The maximum practical achievable limit is 29.4% when taking into account the Auger recombination in the silicon material.<sup>3,4</sup> In the case when the bandgap of the single junction is unconstrained and there are no non-ideal losses, the theoretical limit under the standard AM1.5G illumination<sup>5</sup> is 33.8%, which is far from 100%. The main contributors to this difference are sub-bandgap and thermalization losses. The former results from photons with energy less than the bandgap of the semiconductor in the single-junction solar cell that cannot be absorbed by creating electron-hole pairs and the latter from photons with energy exceeding the bandgap that are absorbed but with their excess energy dissipated as heat.

Multi-junction tandem solar cells involve the stacking of solar cells with different bandgaps (highest on the sun-facing side) allowing each cell to absorb different parts of the solar spectrum more efficiently,

minimizing sub-bandgap and thermalization losses. Figures 1(a) and 1(b) illustrate two configurations for double-junction tandem cells. Figure 1(c) shows the reduction of sub-bandgap and thermalization losses as the number of junctions in a tandem stack increases. The theoretical efficiency limit of multi-junction also increases with the number of junctions from  $\sim 45\%$  for double junction to  $\sim 51\%$  for triple junction and to  $\sim 55\%$  for four-junction tandems as shown in Fig. 1(d).<sup>6</sup> Multi-junction concepts have been implemented for III-V solar cells in the last few decades<sup>7</sup> especially for space applications where the energy conversion efficiency is paramount, outweighing the cost.

A double-junction tandem is the simplest implementation of the multi-junction approach. They can be realized by mechanically stacking the high-bandgap cell on top of the low bandgap cell with the cells operating independently electrically. The total power is the sum of power generated by each cell. This approach involves the least integration effort, allowing cells to be fabricated and optimized independently at the expense of extra wiring and an insulating layer between the cells

incurring extra cost. The insulating layer needs to be chosen to reduce the refractive index mismatch when interfacing with the cells<sup>8</sup> in order to minimize the optical loss from Fresnel reflection. The transparent electrodes also need to have a sufficient lateral conductivity for independent cell operation but will inevitably introduce some level of optical transmission loss.

A monolithically integrated tandem represents the more elegant tandem approach, typically involving the fabrication of the high-bandgap cell directly on the low bandgap cell. This means that fabrication technologies for the top cell must be “bottom-cell compatible” so to not cause any damage during cell processing. The fabrication of interconnection layer(s) is also required but can be made ultra-thin as the layer or the stack is only responsible for vertical (not lateral) carrier transport. This can be via tunneling or recombination layers in the form of carrier selective layers, transparent conductive oxide (TCO), such as indium tin oxide (ITO) or ultra-thin metal.<sup>10,11</sup> As the cells are electrically connected in series, the output voltage of the tandem will

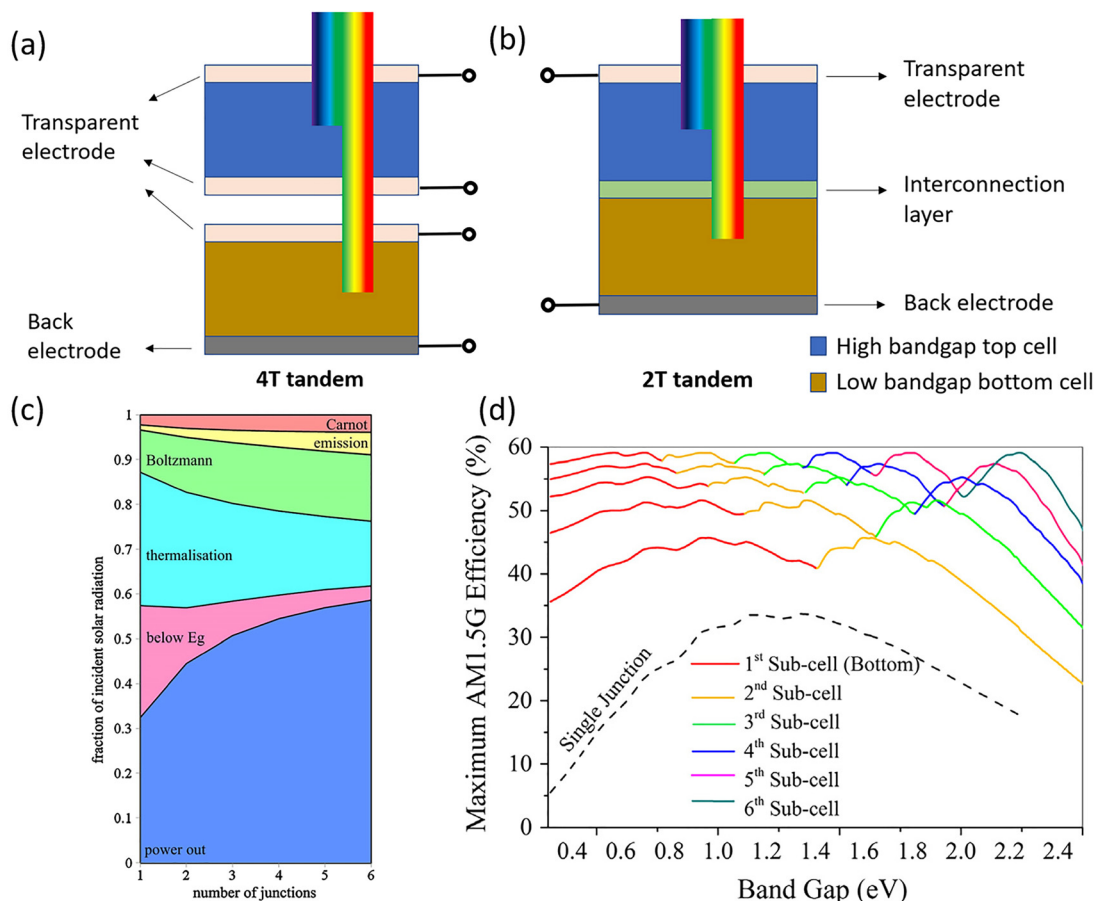


**FIG. 1.** Schematics of two types of two-junction tandem configurations: (a) Four-terminal (4T) mechanically stacked tandem and (b) two terminal (2T) monolithically integrated tandem. (c) Fundamental losses in solar cells as a function of the number of junctions under the AM1.5 solar spectrum.<sup>8</sup> Reproduced with permission from L. C. Hirst and N. Ekins-Daukes, *Prog. Photovoltaics* **19**, 286 (2011). Copyright 2011 John Wiley and Sons, Inc. (d) Maximum efficiency for a bandgap value as part of a multi-junction solar cell stack for cases up to and including six band gaps under the air mass 1.5 global (AM1.5G) standard solar spectrum.<sup>6</sup> Reproduced with permission from Bremner *et al.*, *Sol. Energy* **135**, 750 (2016). Copyright 2016 Elsevier.

be the sum of the voltages of the individual cells. However, the current will be limited by the cell with the least output. This highlights the importance of the individual cell efficiencies for tandems. There is no incentive in stacking an under-performing high-bandgap cell on top of a high efficiency cell “poaching” valuable sunlight from it. Therefore, cell technologies chosen for tandems must be comparable, with similar efficiencies.

Hybrid metal halide perovskite solar cell technology<sup>12</sup> [perovskite crystal structure shown in Fig. 2(a)] has recently emerged as a promising candidate for multi-junction tandems due to the rapid improvement in its power conversion efficiency (PCE) from 3.8% in 2009<sup>13</sup> to the recently certified 25.5% in 2020.<sup>7</sup> The high performance is due to its high external radiative efficiency (ERE) comparable to those of Si and copper indium gallium selenide (CIGS) solar cell technologies.<sup>14</sup> Perovskites have strong optical absorption meaning cells can be prepared as thin films and can be readily fabricated by solution processing. Bandgap can also be tuned (e.g., from 1.20 to 2.3 eV) via compositional engineering. All of these attributes make metal halide perovskites highly desirable for tandem cell applications. Most recently, reports of perovskite–Si,<sup>15</sup> perovskite–CIGS,<sup>16</sup> perovskite–perovskite,<sup>17</sup> and perovskite–organic-photovoltaics (OPV) tandems<sup>18</sup> have demonstrated promising energy conversion efficiencies.

Figure 2(b) shows the efficiency potentials of double-junction perovskite-based tandem solar cells based on the Shockley–Queisser limit calculations assuming the bandgaps listed in the table in Fig. 2 for each subcell. The bandgaps of Si, CIGS, perovskite, and OPV bottom subcells are based on what has been demonstrated or feasible, especially for perovskite and OPV’s.<sup>17,19</sup> The top cell bandgaps are based on the best values that produce the highest tandem cell performance assuming 100% absorption and no non-ideal carrier-recombination in any of the subcells, showing above 40% energy conversion efficiencies are achievable. This shows the great potential for these tandem technologies to overcome the efficiency limits for single-junction cells.

## II. RECENT PROGRESS OF TANDEM SOLAR CELLS USING PEROVSKITES

As discussed above, monolithic tandem cells have the advantages of wiring simplicity, material savings, and reduced optical loss from a much thinner interconnection layer or stack between the subcells compared to the mechanically stacked tandem. Therefore, this review will focus on monolithic tandem designs, which are commercially attractive despite integration challenges, along with other general challenges associated with

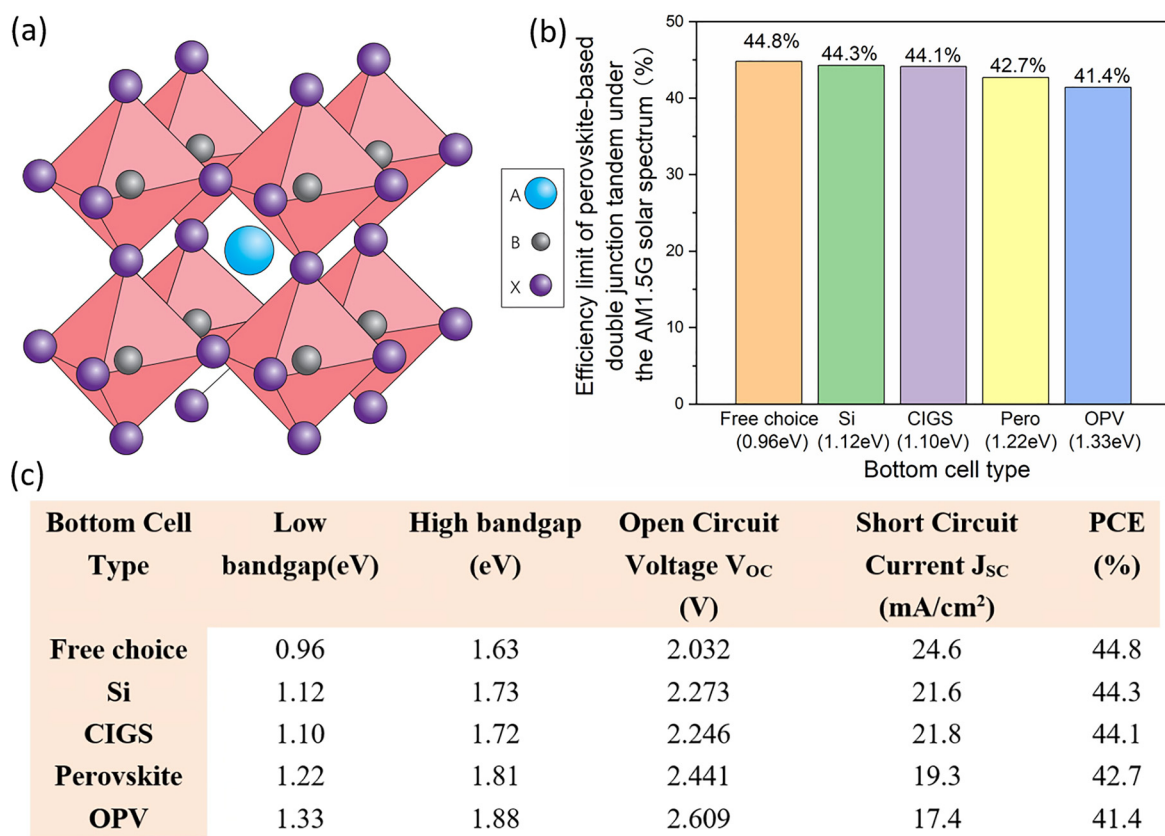


**FIG. 2.** (a) Cubic perovskite crystal structure.<sup>12</sup> Reproduced with permission from Green *et al.*, Nat. Photonics. 8, 506 (2014). Copyright 2014 Springer Nature. Efficiency limit of various perovskite-based double-junction monolithic tandems displayed (b) graphically and (c) listed in tabulated form.

tandems using perovskite which will be discussed below. Figure 3 shows the reported and certified efficiencies of perovskite–Si, perovskite–CIGS, perovskite–perovskite, and perovskite–OPV tandems that can be found in published scientific journals or press releases.<sup>7,15–88</sup> While the numbers are well below the theoretical limits (Fig. 2), the effectiveness of tandems using perovskites is clearly evident by the fact that tandem efficiencies of demonstrated perovskite–Si, perovskite–CIGS, and perovskite–OPV tandems have exceeded the efficiencies of demonstrated single-junction Si, CIGS, and OPV cells (Fig. 3) given that the first perovskite tandem cell demonstration was only in 2015. Past advancements made with these tandems will be reviewed in this article.

Although, at this stage, only the perovskite–Si tandem cell has been demonstrated to exceed the demonstrated performance of single-junction perovskite cells, it is expected that perovskite–perovskite, perovskite–CIGS and perovskite–OPV tandem cells will follow suit in the near term. Challenges and outlook for further efficiency improvements for perovskite tandems will also be outlined in this article guiding future research.

### A. Perovskite–silicon tandem solar cells

As shown in Fig. 4 and Table I, a great progress has been made in the development of high-efficiency monolithic perovskite–Si tandem solar cells since 2015.

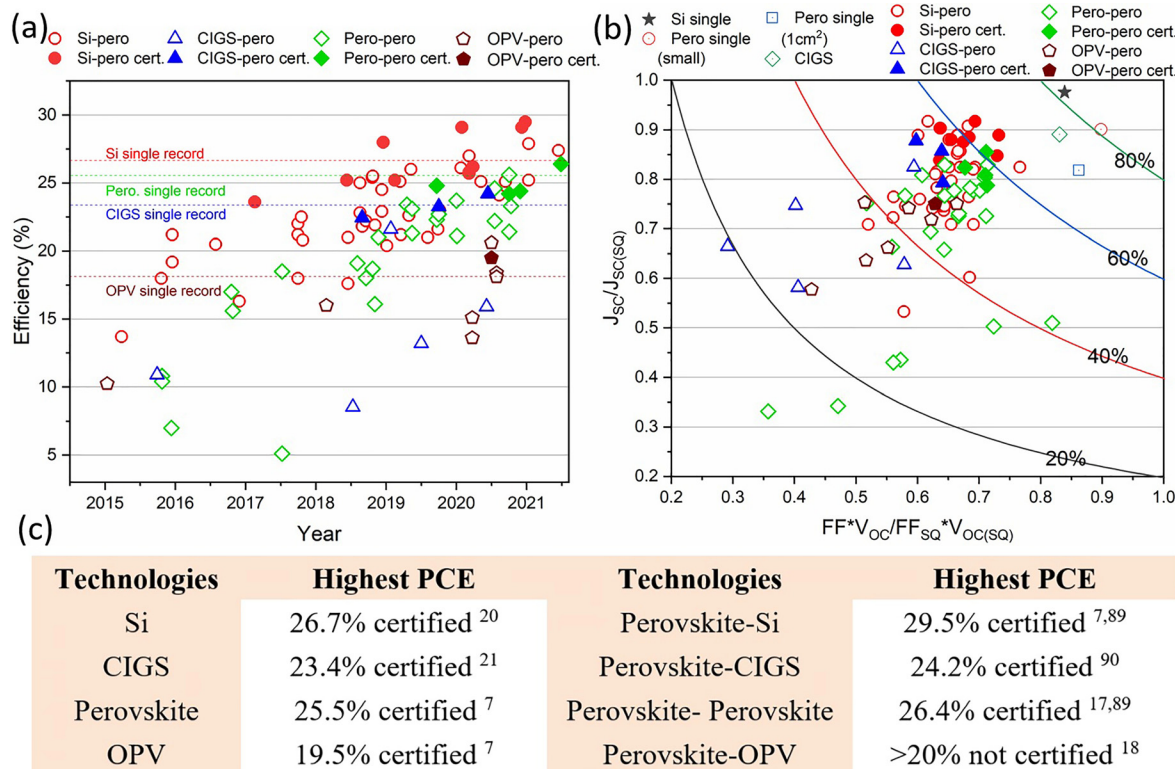


**FIG. 3.** Two-terminal double-junction perovskite tandem solar cells. (a) Evolution of tandem cell energy conversion efficiencies reported.<sup>7,15–84,88,89</sup> (b)  $J_{SC}$  vs  $FF \cdot V_{OC}$  as a percentage of theoretical limits. Solid markers: independently certified results.<sup>7,15–84,88,89</sup> (c) List of record efficiencies of perovskite tandem cells.

Mailoa *et al.*<sup>22</sup> reported the first demonstration of monolithic perovskite–Si tandem in 2015 using homo-junction Si as the bottom cell, a mesoscopic perovskite top cell with a n++ tunneling junction layer for the integrating the two cells. The champion cell achieved a 13.7% PCE on 1 cm<sup>2</sup> with a  $V_{OC}$  of 1.65 V. The first demonstration of monolithic perovskite–Si tandem using a heterojunction silicon bottom cell as the bottom cell was reported by Albrecht *et al.*<sup>23</sup> in late 2015. The champion cell achieved a PCE of 18% and  $V_{OC}$  of 1.78 V. Since then, heterojunction Si cells have been widely used as the bottom cells for laboratory demonstrations (Table I) due to the readily available indium tin oxide (ITO) for top and bottom cell integration and demonstrated high open voltage and therefore efficiency. Nevertheless, homo-junction Si cells especially of PERC or PERL type (where “PE” standards for passivated emitter, “RC” standards for rear contacts, and “RL” standards for rear localized contacts), as bottom cell choice are industrially relevant, since of lower cost than heterojunction Si cells<sup>90</sup> while also having high efficiency, providing an immediate pathway for commercializing perovskite–Si tandems. Due to the absence of an amorphous Si layer found in heterojunction cells, homo-junction cells can withstand higher processing temperature during subsequent perovskite cell fabrication. Relatively few perovskite–Si-homo-junction-cell tandem demonstrations have been reported to date (Table I), meaning there is scope for improvement, such as in further optimization of the front emitter of the Si bottom cell allowing for heavier doping. This is not possible for single-junction Si cells without jeopardizing blue light response, which is no longer absorbed by the Si

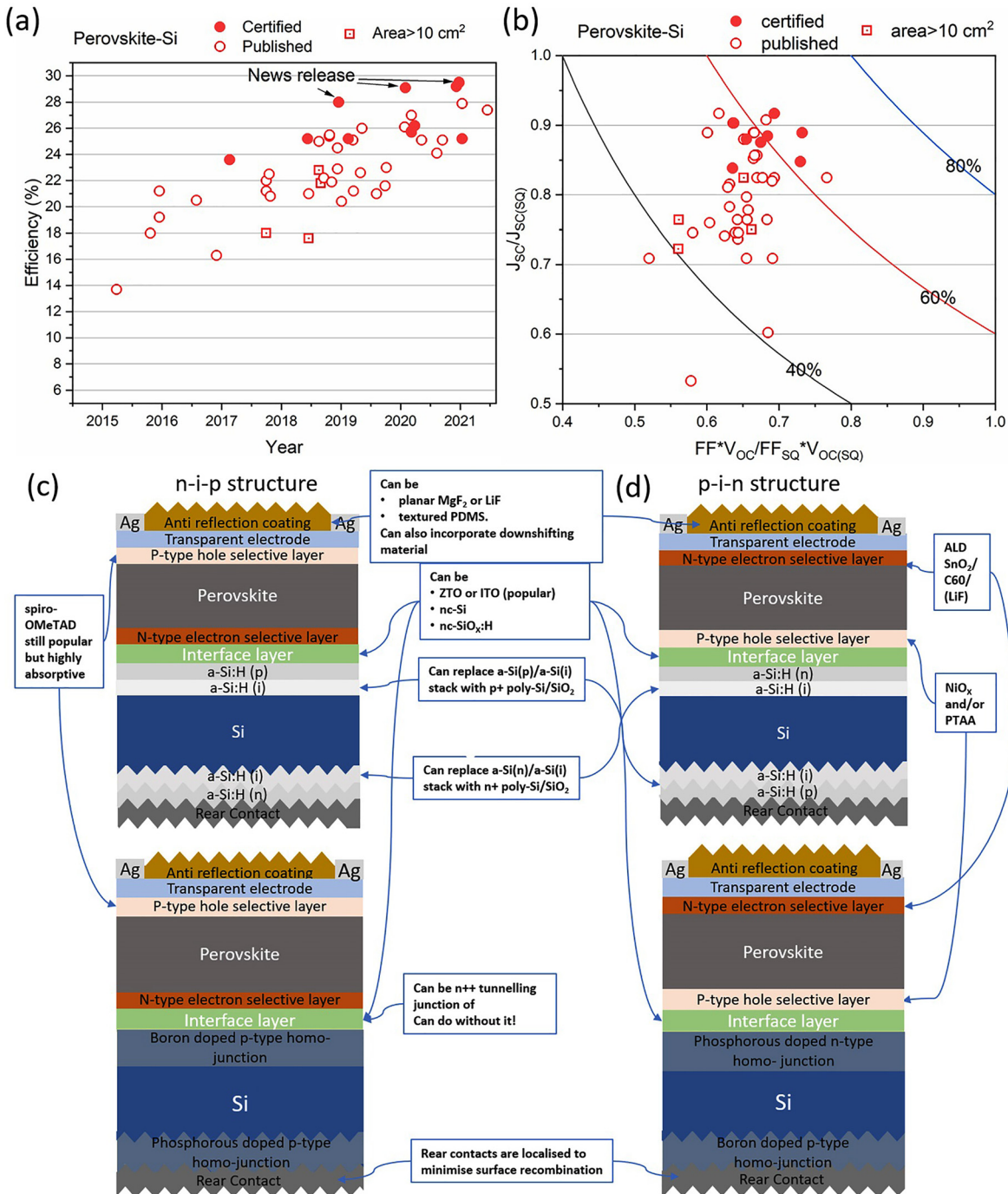


**FIG. 4.** Two terminal perovskite-Si tandem solar cell. (a) Evolution of energy conversion efficiency. (b)  $J_{SC}$  vs  $FF \times V_{OC}$  as a percentage of theoretical limits. (c) and (d) Different types of cell designs contrasting n-i-p vs p-i-n structures and contrasting homo-junction vs hetero-junction Si bottom cells.

bottom cell in a tandem but by the perovskite top cell. Other approaches for further improving the efficiencies of Si bottom cells can also be investigated.<sup>20,91</sup> The lower output current (halved in a two junction) in a tandem also means that previous design restrictions can be relaxed due to lower resistive losses.

In terms of the interface layer between the perovskite and Si sub-cells, ITO with a thickness of 40–120 nm (Refs. 23, 28, 29, 34, 35, 42, 45, 49, and 54) is typically used in earlier works. Thinner layers [e.g., 10–20 nm (Refs. 15, 32, 36, 37, 46, 47, 50, 53, and 85)] result in less parasitic absorption and optical loss. Zinc tin oxide (ZTO),

**TABLE I.** Demonstrated monolithic perovskite–Si tandems. MA =  $\text{CH}_3\text{NH}_3$ , FA =  $\text{HC}(\text{NH}_2)_2$ , SHJ = silicon heterojunction solar cells.

Lower-bandgap bottom cell	Interface	Higher-bandgap top cell	$V_{\text{OC}}$ (V)	$J_{\text{SC}}$ (mA/cm <sup>2</sup> )	FF (%)	Eff. (%)	Area (cm <sup>2</sup> )	Reference
Homo junction (p+ front emitter/n-Si/n++ rear BSF) SHJ [a-Si(p) front/n-Si]	n++Si ITO	mp-TiO <sub>2</sub> /MAPbI <sub>3</sub> /Spiro-OMeTAD/AgNW/LiF ALD SnO <sub>2</sub> /MA <sub>X</sub> FA <sub>1-X</sub> PbI <sub>y</sub> Br <sub>3-Y</sub> /Spiro-OMeTAD/MoO <sub>X</sub> /ITO/LiF	1.58 1.80	11.5 13.0	75 78	13.7 18.0	1.0 0.16	22 23
SHJ (a-Si(p) front / n-Si)	IZO	PCBM/PEIE/MAPbI <sub>3</sub> /Spiro-OMeTAD/ MoO <sub>X</sub> /ITO/IO:H/ARF	1.70 1.69	16.1 15.9	70 78	19.2 21.2	1.22 0.17	24
SHJ [a-Si(p) front/n-Si]	IZO	SnO <sub>2</sub> /PEIE/PCBM/MAPbI <sub>3</sub> /Spiro-OMeTAD/ MoO <sub>X</sub> /IO:H/ITO	1.72	16.4	72	20.5 <sup>a</sup>	1.43	25
Homo junction (p+ front emitter/n-Si/n++ rear BSF) SHJ [a-Si(p) rear/n-Si]	ZTO ITO	Sputtered c-TiO <sub>2</sub> /mp-TiO <sub>2</sub> /MAPbI <sub>3</sub> /Spiro- OMeTAD/MoO <sub>X</sub> /ITO/IO:H/ARF NiO/FA <sub>0.83</sub> Cs <sub>0.17</sub> Pb(I <sub>0.83</sub> Br <sub>0.17</sub> ) <sub>3</sub> /LiF/PC <sub>60</sub> BM/ SnO <sub>2</sub> /ZTO/ITO/Ag/LiF	1.64 1.65	15.3 18.1	65 79	16.3 23.6 <sup>b</sup>	1.43 0.99	26 85
SHJ (a-Si(p) front / n-Si)	nc-Si:H(p+)/ nc-Si:H(n+)	C <sub>60</sub> /Cs <sub>0.19</sub> MA <sub>0.81</sub> PbI <sub>3</sub> /Spiro-OMeTAD/ MoO <sub>X</sub> /IZO/MgF <sub>2</sub>	1.75 1.78 1.77	16.8 16.5 16.5	77 74 65	22.0 <sup>a</sup> 21.2 <sup>a</sup> 18.0 <sup>a</sup>	0.25 1.43 13.0	27
Homo junction p+ front emitter/n-Si/n++ rear BSF)	Al <sub>2</sub> O <sub>3</sub> /SiN <sub>X</sub> /ITO	c-TiO <sub>2</sub> /mp-TiO <sub>2</sub> / Cs <sub>0.07</sub> Rb <sub>0.03</sub> FA <sub>0.765</sub> MA <sub>0.135</sub> PbI <sub>2.55</sub> Br <sub>0.45</sub> /Spiro- OMeTAD/MoO <sub>X</sub> /IZO/ARF	1.75	17.6	74	22.5 <sup>a</sup>	1.0	28
SHJ [a-Si(p) front/n-Si]	ITO	SnO <sub>2</sub> /MA <sub>0.37</sub> FA <sub>0.48</sub> Cs <sub>0.15</sub> PbI <sub>2.01</sub> Br <sub>0.99</sub> /Spiro- OMeTAD/MoO <sub>X</sub> /ITO/LiF	1.70	15.3	79	20.6	0.03	29
Homo junction (p+ front emitter /n-Si/n++ rear PERL)	None	SnO <sub>2</sub> /MAPbI <sub>3</sub> /Spiro-OMeTAD/MoO <sub>3</sub> /ITO/ ARF	1.68 1.69	16.1 15.6	78 68	20.5 <sup>a</sup> 17.1 <sup>a</sup>	4.0 16.0	30
SHJ [a-Si(p) rear/n-Si]	nc-Si:H(n+)/ nc-Si:H(p+)	Spiro-TTB/Cs <sub>X</sub> FA <sub>1-X</sub> Pb(I,Br) <sub>3</sub> /LiF/C <sub>60</sub> /SnO <sub>2</sub> / IZO/Ag/MgF <sub>2</sub>	1.79	19.5	73	25.2 <sup>a,b</sup>	1.42	31
SHJ [a-Si(p) rear/n-Si]	ITO	PTAA/FA <sub>0.83</sub> Cs <sub>0.17</sub> Pb(I <sub>0.83</sub> Br <sub>0.17</sub> ) <sub>3</sub> /C <sub>60</sub> /SnO <sub>2</sub> / ZTO/ITO/Ag/ PDMS	1.77	18.4	77	25.0	1.0	32
Homo junction (p+ front emitter /n-Si/n++ rear PERL)	None	SnO <sub>2</sub> /(FAPbI <sub>3</sub> ) <sub>0.83</sub> (MAPbI <sub>3</sub> ) <sub>0.17</sub> /Spiro- OMeTAD/MoO <sub>3</sub> /ITO/ARF	1.74	16.2	78	21.8 <sup>a</sup>	16.0	33
SHJ [nc-SiO <sub>X</sub> :H(p) front/n-Si]	ITO	SnO <sub>2</sub> /MAFACsPbIBr/Spiro-OMeTAD/ MoO <sub>X</sub> /ITO/ARC	1.78	17.8	75	22.8 <sup>b</sup>	0.13	34
SHJ [a-Si(p) front/n-Si]	ITO	SnO <sub>2</sub> /FA <sub>0.5</sub> MA <sub>0.38</sub> Cs <sub>0.12</sub> PbI <sub>2.04</sub> Br <sub>0.96</sub> /Spiro- OMeTAD/MoO <sub>X</sub> /ITO	1.66	16.5	81	22.2	0.06	35
SHJ [a-Si(p) rear/n-Si]	ITO	PTAA/Cs <sub>0.15</sub> (FA <sub>0.83</sub> MA <sub>0.17</sub> ) <sub>0.85</sub> Pb(I <sub>0.8</sub> Br <sub>0.2</sub> ) <sub>3</sub> / ICBA/C <sub>60</sub> /SnO <sub>2</sub> /IZO/Cu/MgF <sub>2</sub>	1.80	17.8	79	25.4	0.42	36
SHJ [a-Si(p) rear/n-Si/nc- SiO <sub>X</sub> :H(n) FSF]	ITO	PTAA/Cs <sub>0.05</sub> (FA <sub>0.83</sub> MA <sub>0.17</sub> ) <sub>0.95</sub> Pb(I <sub>0.83</sub> Br <sub>0.17</sub> ) <sub>3</sub> / ICBA/C <sub>60</sub> /SnO <sub>2</sub> /IZO/Ag/PDMS	1.76	18.5	78	25.5	0.77	37
?	?	?	1.80	19.8	79	28.0 <sup>b</sup>	1.03	88
SHJ [nc-SiO <sub>X</sub> :H(p) front/n-Si]	ITO	SnO <sub>2</sub> /MAFACsPbIBr/Spiro-OMeTAD/ MoO <sub>X</sub> /ITO/Au/PDMS	1.75	16.9	74	21.9	0.13	40
SHJ [poly-Si (p+) front/n-Si]	None	c-TiO <sub>2</sub> /mp-TiO <sub>2</sub> / PMMA/PCBM/ Cs <sub>0.05</sub> Rb <sub>0.05</sub> FA <sub>0.765</sub> MA <sub>0.135</sub> PbI <sub>2.55</sub> Br <sub>0.45</sub> /PTAA	1.76	17.8	78	24.5	1.0	41

TABLE I. (Continued.)

Lower-bandgap bottom cell	Interface	Higher-bandgap top cell	V <sub>OC</sub> (V)	J <sub>SC</sub> (mA/cm <sup>2</sup> )	FF (%)	Eff. (%)	Area (cm <sup>2</sup> )	Reference
Homo junction (p+ front emitter/n-Si/n+ rear BSF)	None	for SHJ or Spiro-OMeTAD for homo junction Si/MoO <sub>x</sub> /IZO/Au/PDMS	1.70	17.2	79	22.9 <sup>a</sup>	1.0	
SHJ [a-Si(p) rear/n-Si]	ITO	SnO <sub>2</sub> /MAFACsPbIBr/Spiro-OMeTAD/ MoO <sub>x</sub> /ITO/Au	1.83	16.0	70	20.4	0.13	42
SHJ [nc-SiO <sub>x</sub> :H(n) front/n-Si]	ITO	F4-TCNQ:polyTPD/ Cs0.05(FA0.83MA0.17)0.95Pb(I <sub>1-x</sub> Br <sub>x</sub> ) <sub>3</sub> /ETL/ Buffer/ITO/Ag/ARC	1.79	19.0	75	25.2 <sup>b</sup>	1.0	43
SHJ [nc-SiC(n) front/SiO <sub>x</sub> /p-Si]	nc-Si:H (p+)	Spiro-TTB/CsFAPbIBr/LiF/C <sub>60</sub> /SnO <sub>2</sub> /IZO/Ag/ MgF <sub>2</sub>	1.74	19.5	75	25.1	1.42	44
Homo junction (n+ front emitter/p-Si/rear Al-BSF)	ITO	PTAA/(FAPbI <sub>3</sub> ) <sub>0.8</sub> (MAPbBr <sub>3</sub> ) <sub>0.2</sub> /PCBM/ZnO/ IZO)/Ag/LiF	1.65	16.1	80	21.2	0.27	45
SHJ [a-Si(p) rear/n-Si]	ITO	NiO/Cs <sub>0.17</sub> FA <sub>0.83</sub> PbI <sub>0.83</sub> Br <sub>0.17</sub> /C <sub>60</sub> /SnO <sub>2</sub> /ITO/ Ag/MgF <sub>2</sub>	1.72	17.5	75	22.6	57.4	46
SHJ (a-Si(p) rear / n-Si)	ITO	PTAA/Cs <sub>0.05</sub> (MA <sub>0.83</sub> FA <sub>0.17</sub> )Pb(I <sub>0.83</sub> Br <sub>0.17</sub> ) <sub>3</sub> / C <sub>60</sub> /SnO <sub>2</sub> /IZO/Ag/LiF	1.77	19.2	77	26.0	0.77	47
SHJ [a-Si(p) front/n-Si]	None	SnO <sub>2</sub> /(FAPbI <sub>3</sub> ) <sub>0.83</sub> (MAPbI <sub>3</sub> ) <sub>0.17</sub> /Spiro- OMeTAD/MoO <sub>3</sub> /ITO/Ag/ (Ba,Sr) <sub>2</sub> SiO <sub>4</sub> :Eu <sup>2+</sup> :PDMS	1.73	16.5	81	23.0 <sup>a</sup>	4.0	92
SHJ [a-Si(p) front/n-Si]	ITO	TiO <sub>2</sub> /mp-TiO <sub>2</sub> /PCBM:PMMA/ FA <sub>0.75</sub> Cs <sub>0.25</sub> Pb(I <sub>0.8</sub> Br <sub>0.2</sub> ) <sub>3</sub> /Spiro-OMeTAD/ ITO/MgF <sub>2</sub>	1.84	15.3	77	21.6 <sup>a</sup>	0.249	49
SHJ [a-Si(p+) rear/n-Si]	ITO	PTAA/Cs <sub>0.1</sub> MA <sub>0.9</sub> Pb(I <sub>0.9</sub> Br <sub>0.1</sub> ) <sub>3</sub> /C <sub>60</sub> /SnO <sub>2</sub> / ITO/Ag/PDMS	1.82	19.2	75	26.1 <sup>a</sup>	0.42	50
SHJ [a-Si(p+) rear/n-Si]	InO <sub>x</sub>	NiO <sub>x</sub> /Cs <sub>0.05</sub> MA <sub>0.15</sub> FA <sub>0.8</sub> PbI <sub>2.25</sub> Br <sub>0.75</sub> /LiF/C <sub>60</sub> / SnO <sub>2</sub> /IZO/Ag/MgF <sub>2</sub>	1.78	19.0	75	25.7 <sup>b</sup>	0.832	51
SHJ (a-Si(p+) rear/ n-Si)	ITO	NiO <sub>x</sub> /Poly-TPD/PFN/Cs <sub>x</sub> FA <sub>1-x</sub> PbI <sub>y</sub> Br <sub>1-y</sub> +MAPbCl <sub>3</sub> /LiF/C <sub>60</sub> /SnO <sub>2</sub> /ZTO/IZO/Ag/ PDMS	1.87	19.1	75	27.0 <sup>a</sup>	1.0	52
SHJ [a-Si(p+) rear/n-Si]	ITO	PTAA/ PEA(I <sub>0.25</sub> SCN <sub>0.75</sub> ):FA <sub>0.65</sub> MA <sub>0.20</sub> Cs <sub>0.15</sub> Pb(I <sub>0.8</sub> Br <sub>0.2</sub> ) <sub>3</sub> /C <sub>60</sub> /PEIE/ITO/Ag	1.82	18.9	76	26.2 <sup>b</sup>	1.001	53
SHJ [a-Si(p+) rear/n-Si]	ITO	PTAA/PFN/ FA <sub>0.75</sub> Cs <sub>0.25</sub> Pb(I <sub>0.8</sub> Br <sub>0.2</sub> ) <sub>3</sub> /C <sub>60</sub> / SnO <sub>x</sub> /ITO/MgF <sub>2</sub>	1.77	17.7	80	25.1 <sup>b</sup>	0.25	54
SHJ [a-Si(p+) rear/n-Si/a-Si(i)/ a-Si:H(n)]	ITO	NiOx/PTAA/(MAPb(I <sub>0.75</sub> Br <sub>0.25</sub> ) <sub>3</sub> /C <sub>60</sub> /SnO <sub>2</sub> / IZO/MgF <sub>2</sub>	1.76	19.2	70	24.1 <sup>a</sup>	1.0	55
SHJ [a-Si(p+) rear/n-Si/a-Si(i)/ nc-SiO <sub>x</sub> (n)]	Nc-Si:H(n+)/Spiro-TTB	Spiro-TTB/FACsMAPbI <sub>3-x</sub> Br <sub>x</sub> /C <sub>60</sub> /SnO <sub>2</sub> /IZO	1.73	19.8	73	25.1	1.0	56
SHJ [a-Si(p+) rear/n-Si/a-Si(i)/ nc-SiO <sub>x</sub> (n)]	ITO	PTAA(or SAM)/ Cs <sub>0.05</sub> (FA <sub>0.77</sub> MA <sub>0.23</sub> ) <sub>0.95</sub> Pb(I <sub>0.77</sub> Br <sub>0.23</sub> ) <sub>3</sub> /LiF/ C <sub>60</sub> /SnO <sub>2</sub> /IZO/LiF	1.90	19.3	79	29.2 <sup>b</sup>	1.06	15

TABLE I. (Continued.)

Lower-bandgap bottom cell	Interface	Higher-bandgap top cell	$V_{OC}$ (V)	$J_{SC}$ (mA/cm <sup>2</sup> )	FF (%)	Eff. (%)	Area (cm <sup>2</sup> )	Reference
?	?	NiO <sub>x</sub> /FACsMAPbI <sub>3-x</sub> Br <sub>x</sub> /C <sub>60</sub> /SnO <sub>2</sub> /IZO/MgF <sub>2</sub>	1.88	20.26	77	29.5 <sup>b</sup>	1.212	100
SHJ [a-Si(p+) rear/n-Si/a-Si:H(i)/nc-Si(n)]	ITO	2PACz/C <sub>60</sub> 0.05(FA <sub>0.77</sub> MA <sub>0.23</sub> ) <sub>0.95</sub> Pb(I <sub>0.77</sub> Br <sub>0.23</sub> ) <sub>3</sub> /LiF/C <sub>60</sub> /SnO <sub>2</sub> /IZO/LiF	1.94	17.8	81	27.9	1.0	86
SHJ [a-Si(p+) rear/n-Si(a-SiOx(n))]	ITO	SAM/C <sub>60</sub> 0.15MA <sub>0.15</sub> F <sub>A0.70</sub> Pb(I <sub>0.80</sub> Br <sub>0.20</sub> ) <sub>3</sub> /C <sub>60</sub> /SnO <sub>2</sub> /IZO/MgF <sub>2</sub>	1.84	19.6	76	27.4	1.03	87
SHJ [a-Si(p+) rear/n-Si/a-Si(i)/a-Si:H(n)]	ITO							

<sup>a</sup>Steady-state.<sup>b</sup>Certified or independently verified.

nanocrystalline silicon (nc-Si), and nanocrystalline silicon oxide inter-layers are just as effective or even better optically as reported by Werner *et al.* in 2016,<sup>26</sup> Sahli *et al.* in 2017<sup>27</sup>, and Mazzarella *et al.* in 2019,<sup>43</sup> respectively. In fact, work by Zheng *et al.*<sup>30,33,92</sup> and Shen *et al.*<sup>41</sup> demonstrated that transparent conductive oxide, such as ITO, is not a prerequisite for interfacing top and bottom cells in perovskite-Si-homo-junction tandems. They showed that both solution-processed SnO<sub>2</sub> and TiO<sub>2</sub> deposited by atomic layer deposition (ALD) can act as electron transport layers for the perovskite top cell as well as recombination layers for the perovskite-Si interface. Zheng *et al.*<sup>30,92</sup> found that their interface-TCO-free tandems are suitable for large area cells which have a very narrow distribution of fill factor values. This is due to the limited lateral conductivity (otherwise present in TCO) in the SnO<sub>2</sub> layer thereby localizing any undesirable shunting related effects. A similar effect using nanocrystalline Si as a recombination junction with poor lateral conductivity for localizing shunting is also reported by Sahli *et al.*<sup>27</sup> Integration approaches suitable for PERC or PERL cells are also suitable for newer type of homo-junction cells with poly-Si with tunnel oxide passivated contacts.<sup>41</sup>

In terms of cell polarity, the n-i-p structure (where “n” is at the bottom and “p” is at the top sun facing side) has been the most popular in the early stages of tandem cell development due to the proven process for perovskite cell fabrication where the electron transport layer (e.g., TiO<sub>2</sub> of SnO<sub>2</sub>) is fabricated first and hole transport layer (HTL) such as 2,2',7,7'-Tetrakis[N,N-di(4-methoxyphenyl)amino]-9,9'-spirobifluorene (spiro-OMeTAD) is fabricated after perovskite deposition. However, spiro-OMeTAD has a very high parasitic absorption and the presence of MoO<sub>3</sub> (necessary for protecting the spiro-OMeTAD and the underlying layers from damage caused by sputtering which is typically used to deposit the top transparent conductive oxide electrode) causes Fresnel reflection and therefore optical losses.<sup>30</sup> One way of circumventing this is to replace the spiro-OMeTAD layer with a less absorptive layer although, so far, with little successes (Table I). Another way is to apply down-shifting material on the top surface of the cell, e.g., attaching a thin polydimethylsiloxane (PDMS) layer incorporated with (Ba,Sr)<sub>2</sub>SiO<sub>4</sub>:Eu<sup>2+</sup>.<sup>92</sup> Ultra violet (UV) light that is typically absorbed by the spiro-OMeTAD layer is downshifted to wavelengths absorbable by the perovskite layer for electrical energy generation. The p-i-n structure (where “p” is at the bottom and “n” is at the top sun facing side) has been shown to overcome the short comings of the n-i-p structure for perovskite-Si tandems. The first tandem demonstration with such a polarity was reported by Bush *et al.*<sup>85</sup> in 2017. The champion cell had a relatively high  $J_{SC}$  of 18.1 mA/cm<sup>2</sup> at the time reporting and achieved a certified efficiency of 23.6%. The typical hole transport layer, which is fabricated before the deposition of perovskite absorber in a p-i-n perovskite cell, is typically NiO<sub>x</sub> or poly[bis(4-phenyl)(2,4,6-trimethylphenyl)-amine] (PTAA) (Table I). The electron-hole transport layer stack (on top of the perovskite absorber) in a p-i-n perovskite cell is typically (LiF)/C<sub>60</sub>/ALD SnO<sub>2</sub> in perovskite-Si<sup>15,25,32,36,37,43–45,50–52,54–57</sup> and in perovskite-CIGS<sup>59,60</sup> tandem solar cells.

In terms of maximizing the current output, MgF<sub>2</sub><sup>27</sup> and LiF<sup>85</sup> can be applied onto the top of the tandem cell to reduce reflection. Si, as an indirect bandgap semiconductor, has a lower absorption coefficient than perovskites<sup>12</sup> requiring light trapping for maximizing optical path length for light absorption, especially for the long-wavelength light. Texturing is effective in this regard. One way of achieving this is

to apply a textured coating such as a textured thin PDMS on the top surface of a perovskite–Si tandem cell. The advantage of using PDMS is that it is relatively easy to control its thickness (to sub-millimeter<sup>92</sup>) to incorporate luminescent materials, such as downshifters for optical management<sup>30</sup> and to mold its surface to replicate different kinds of texturing, such as pyramidal<sup>40</sup> or rose petal surface.<sup>30</sup>  $J_{SC}$  in the range of 15.6–18.4 mA/cm<sup>2</sup> has been achieved using this approach.

Another way to achieve texturing is to texture the Si cell surface directly, which is routinely done for commercial Si cells. The advantage of this approach is that mass-produced Si cells are ready to be used for tandems without altering standard manufacturing processes. However, textured surface poses a challenge to perovskite solar cell fabrication where a conformal coating is desired<sup>93</sup> (Fig. 5). The first work that overcame this challenge was reported by Sahli *et al.*<sup>31</sup> in 2018 who used a two-step sequential deposition method (PbI<sub>2</sub> evaporation and MAI solution spin coating) to fabricate a conformal perovskite layer. The champion cell achieved a certified efficiency of 25.2% and  $J_{SC}$  of 19.5 mA/cm<sup>2</sup> for 1.42 cm<sup>2</sup> area. More recently, three works<sup>50,51,55</sup> have further demonstrated the viability of solution processing for achieving full coverage of perovskite over textured Si surface (where the troughs of the texture are filled) especially when the texture feature size is reduced down to  $\sim 1\text{ }\mu\text{m}$ . These processing methods include blade coating,<sup>50</sup> spin coating,<sup>51</sup> and slot-die-coating<sup>55</sup> (Fig. 5), and tandem cells demonstrated were 26.1%, 25.7% (certified), and 24.1%, efficient, respectively, with  $J_{SC}$  in the range of 19.0–19.2 mA/cm<sup>2</sup>.

Another consideration in terms of the optical performance of tandem cells is the change in solar spectrum content during the day and throughout the year. This causes individual cells to produce less than ideal current output under “non-ideal” or “non-standard” illumination conditions especially when the spectrum is “red-rich” or “blue-rich” depending on the diffuse-direct sunlight composition. The underperforming subcell will limit the output current of the other cell in the tandem due to the cells being connected in series in a two-terminal monolithic configuration. This effect has been modeled by M. T. Hörantner and H. J. Snaith,<sup>94</sup> and the conclusion is that the efficiency of the tandem cell is not significantly “de-rated” by real-world spectral variations. Furthermore, it is possible to optimize tandem solar cell stacks for a specific location for maximizing energy yield and therefore leveled cost of electricity.

Recently, outdoor testing of two terminal perovskite–Si tandem solar cell has been conducted by Aydin *et al.*<sup>56</sup> They found that it was not the spectral content but the temperature dependence of both the silicon and perovskite bandgaps that impacted current performance. The bandgap of Si bottom cell drops with the increasing temperature due to the increased energy of the electrons and weakened interatomic bonds<sup>95</sup> at elevated temperature. This is typical for tetrahedrally coordinated semiconductors as well.<sup>96</sup> However, perovskites have an opposite trend—the bandgap increases with temperature.<sup>96</sup> This is due to the antibonding nature of the highest energy valence band states [e.g., Pb(6s)/I(5p) for MAPbI<sub>3</sub>].<sup>97</sup> These opposite trends in terms of

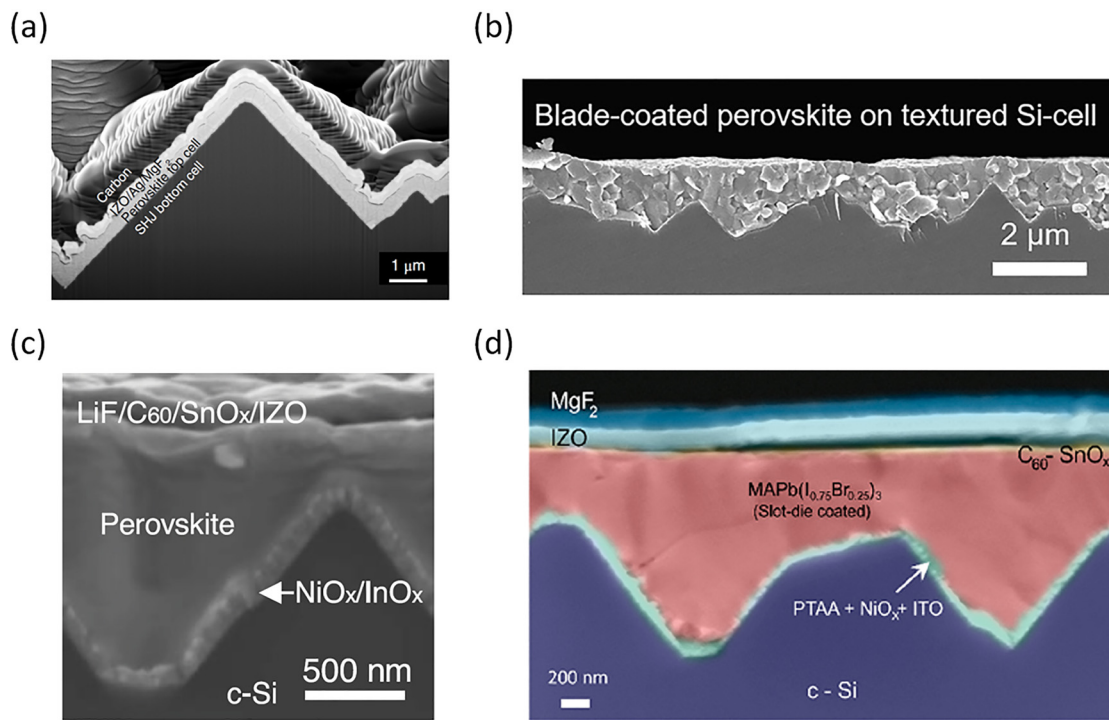


**FIG. 5.** Conformal or full coverage perovskite on textured Si surface achieved by (a) two-step sequential deposition method: PbI<sub>2</sub> evaporation followed by MAI solution spin coating.<sup>31</sup> Reproduced with permission from Sahli *et al.*, Nat. Mater. **17**, 820 (2018). Copyright 2014 Springer Nature. (b) Blade coating.<sup>50</sup> Reproduced with permission from Chen *et al.*, Joule **4**, 850 (2020). Copyright 2020 Elsevier. (c) Spin coating;<sup>51</sup> Reproduced with permission from Hou *et al.*, Science **367**, 1135 (2020). Copyright 2020 American Association for the Advancement of Science, and (d) slot-die-coating;<sup>55</sup> Reproduced with permission from Subbiah *et al.*, ACS Energy Lett. **5**, 3034 (2020). Copyright 2020 American Chemical Society.

bandgaps for the top and bottom cells mean tandems that are optimized at standard test conditions do not necessarily produce matched current outputs in the field. Aydin *et al.* recommended the use of perovskites with bandgap smaller than 1.68 eV favoring bromide-lean perovskites as the top cell choice for field conditions where operational temperatures are higher than 55 °C.

In terms of future improvements, it is clear that  $J_{SC}$  of the state-of-the-art perovskite–Si tandem cells have already reached very high values—90% of the theoretical limit at  $21.6 \text{ mA/cm}^2$  [Fig. 4(b)]. However, there is still room for improvement especially for large area cells, given the growing interest (with a  $13 \text{ cm}^2$  tandem reported in 2017,<sup>27</sup> a  $16 \text{ cm}^2$  tandem reported in 2018<sup>30,92</sup> and a  $57 \text{ cm}^2$  reported in 2019<sup>46</sup> as well as the 6-in. square tandem mentioned in a 2018 press release<sup>88</sup>) This will require a better metal grid design to minimize shading<sup>33</sup> and the development of scalable deposition method (a move away from spin coating), not just for high-quality large-area perovskite films<sup>33,98,99</sup> but also for uniform transport and interface layers.

While it is encouraging that the record efficiency of perovskite–Si tandem at 29.5% (certified) has surpassed the record efficiency of Si

single-junction cell at 26.7% (certified) (Fig. 6), it is clear that  $V_{OC}$  and FF of demonstrated tandems still lag behind their single-junction counterparts. The products of  $V_{OC}$  and FF of perovskite–Si tandem cells are at most 70% of the theoretical limit [Fig. 4(b)] while  $V_{OC} \times \text{FF}$  of the best single-junction Si cell and the best (1.52 eV) single-junction perovskite cells are between 80% and 90% [Fig. 3(b)]. This is because the FF of tandem cells are still less than ideal. Only 5 out of 38 perovskite–Si tandem cells demonstrated have  $\text{FF} \geq 80\%$  indicating a room for improvement especially with the interfacing of the subcells. In terms of  $V_{OC}$ , the success of tandems relies heavily on the voltage output of the top higher-bandgap cell (Table in Fig. 2) as the voltage output of the lower-bandgap cell has less scope for further improvement. Later in this review under Sec. II F, we will review the progress of high-bandgap perovskite solar cells and opportunities for further improvement—critical to the success of perovskite multi-junction tandems.

## B. Perovskite–CIGS tandem solar cells

CIGS is a well-established thin-film photovoltaic technology. While the CIGS bandgap is tunable, the state-of-the-art cells already

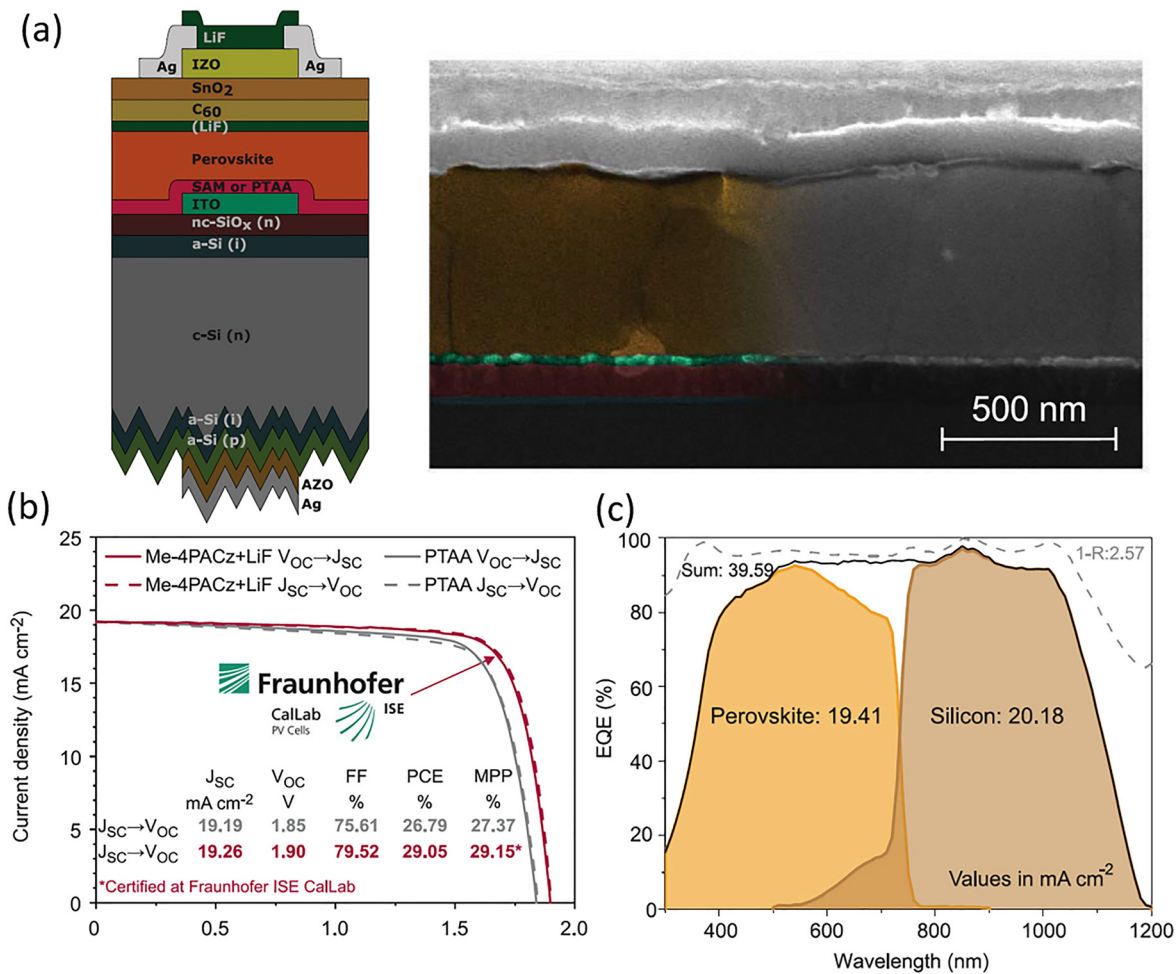


**FIG. 6.** (a) Cell structure, (b) current density–voltage curve, and (c) external quantum efficiency of record monolithic perovskite–Si tandem.<sup>15</sup> Reproduced with permission from Al-Ashouri *et al.*, Science **370**, 1300 (2020). Copyright 2020 American Association for the Advancement of Science.

have a bandgap of 1.08 eV,<sup>21</sup> which is suitably low for them to act as bottom cells for perovskite tandems. Aligning with the standard polarity of a typical CIGS cell,<sup>101</sup> p-i-n cell structure is normally required for the perovskite top cell in a tandem [Fig. 7(c)]. The first demonstration of monolithic perovskite–CIGS tandem was reported by Todorov *et al.*<sup>102</sup> in 2015 [Fig. 7(a)]. The CIGS cell was fabricated by a solution process such that its bandgap could be tuned to 1.04 eV and the perovskite top cell was fabricated by a vapor-assisted process with *in situ* monitoring such that its bandgap could be tuned [Fig. 8(a)]. ZnO, which is typically part of a CIGS cell, was removed, which was believed to be the cause of perovskite instability. The champion cell achieved a PCE of 10.9% and  $V_{OC}$  of 1.45 V. However, it is clear that the bottom CIGS cell performance was inferior, thereby limiting the performance of the tandem.

After a long gap of 3 years, Han *et al.*<sup>16</sup> in 2018 reported a certified 22.4% efficient perovskite–CIGS tandem with some cell design improvements. First of all, the ZnO in the CIGS cell was reinstated. While the long-term cell stability is an ongoing research focus, the cells were stable enough for certification measurements. Second, CIGS by physical deposition was used for the bottom cell which produced higher performance, with a trade-off of film roughness hindering subsequent perovskite cell fabrication. This problem was overcome by chemical mechanical polishing of the ITO layer that capped the BZO/CIGS cell [Fig. 8(b)]. The ITO layer was deposited to be intentionally thick (300 nm) and then polished down to 40 nm without significantly jeopardizing cell efficiency (decreased from 18.7% to 16.8%). However, polishing is a costly process for commercial production.

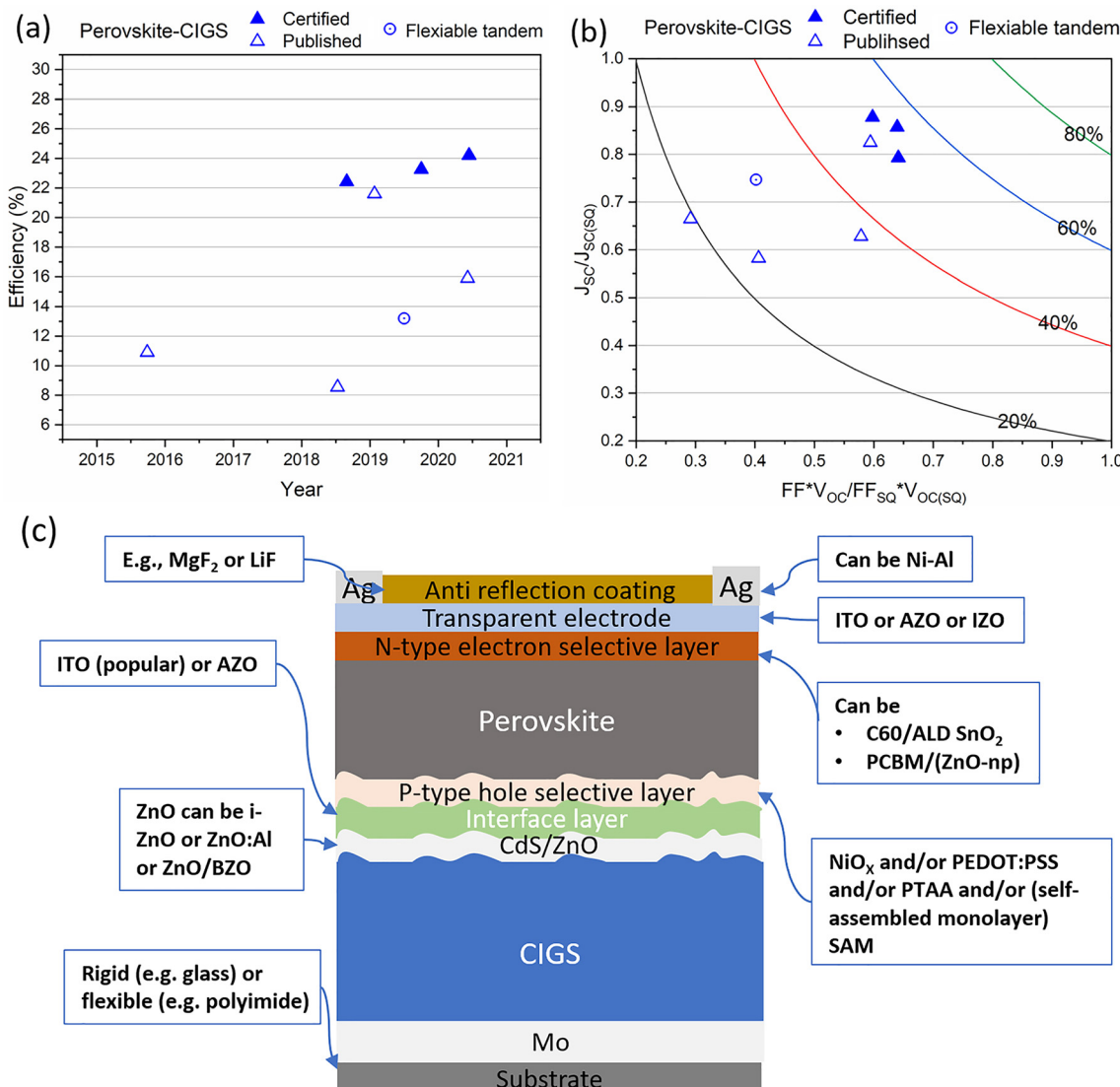
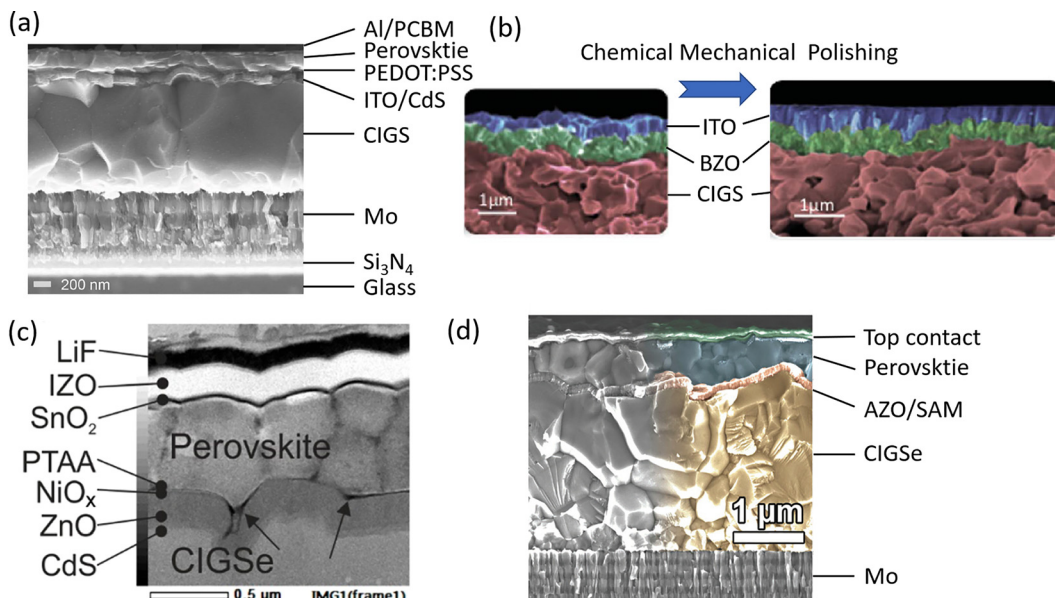


FIG. 7. Two terminal perovskite–CIGS tandem solar cell. (a) Evolution of energy conversion efficiency. (b)  $J_{SC}$  vs  $FF \times V_{OC}$  as a percentage of theoretical limits. (c) Cell design options.



**FIG. 8.** Various fabrication methods and cell designs for achieving perovskite–CIGS monolithic tandem solar cell. (a) Perovskite fabricated by vapor-assisted process on solution processed CIGS.<sup>58</sup> Reproduced with permission from Todorov *et al.*, *Adv. Energy Mater.* **5**, 1500799 (2015). Copyright 2015 John Wiley and Sons, Inc. (b) Chemical mechanical polish to achieve smooth bottom CIGS cell for top perovskite cell fabrication.<sup>16</sup> Reproduced with permission from Han *et al.*, *Science* **361**, 904 (2018). Copyright 2018 American Association for the Advancement of Science. (c) Bilayer  $\text{NiO}_x/\text{PTAA}$  hole transport layer design to achieve conformal coating and efficient charge transport.<sup>59</sup> Reproduced with permission from Jost *et al.*, *ACS Energy Lett.* **4**, 583 (2019). Copyright 2019 American Chemical Society. (d) Solution processed self-assembling monolayers as hole transport layer without requiring ALD to achieve conformal coating.<sup>60</sup> Reproduced with permission from Al-Ashouri *et al.*, *Energy Environ. Sci.* **12**, 3356 (2019). Copyright 2019 Author(s), licensed under a Creative Commons Attribution 3.0 Unported License.

In early 2019, Jost *et al.*<sup>59</sup> from Albrecht’s group reported a perovskite top cell design that is compatible with rough CIGS cell surfaces without requiring polishing. The perovskite top cell utilized a  $\text{NiO}_x/\text{PTAA}$  bilayer as the hole transport layer. The  $\text{NiO}_x$  layer deposited by ALD forms a conformal coating on the CIGS cell and therefore prevents shunting. Instead of a 300 °C post anneal to improve  $\text{NiO}_x$  conductivity (which will adversely affect the CIGSe cell performance due to inter-diffusion at the CIGSe/CdS interface), a PTAA layer is deposited to aid the carrier transport [Fig. 8(c)]. A 21.6% steady-state efficiency was achieved on 0.8 cm<sup>2</sup> area. In the second half of 2019, Al-Ashouri *et al.*<sup>60</sup> also from Albrecht’s group further improved the perovskite cell design focusing on the hole transport layer that is solution processed without the need for ALD. In their work, self-assembling monolayers (SAMs) in the form MeO-2PACz were synthesized and deposited either by spin coating (multiple times) or dip coating to form a conformal coating on the ZnO-capped rough CIGS bottom cell [Fig. 8(d)]. The champion CIGS-perovskite tandem device produced a certified efficiency 23.3% on 1 cm<sup>2</sup> area. The major performance improvement came from high current output.

In early 2020, Jost *et al.* from the same group<sup>63</sup> reported a new certified record efficiency of perovskite–CIGS tandem with 24.2% efficiency. While the cell structure was essentially unchanged from that last reported by Al-Ashouri *et al.*,<sup>40</sup> PEAI was incorporated into the  $\text{Cs}_{0.05}(\text{MA}_{0.23}\text{FA}_{0.77})\text{Pb}_{1.1}(\text{I}_{0.77}\text{B}_{0.23})_3$  perovskite and 1 nm LiF was deposited onto the perovskite layer to reduce interface recombination, producing a high  $V_{OC}$  value of 1.77 V. Another interesting work by Fu *et al.*<sup>61</sup> involved a proof-of-concept of a flexible perovskite–CIGS

tandem on 30 μm polyimide foil with an efficiency of 13.2% and  $V_{OC}$  of 1.75 V. Further work has been suggested by the authors to improve efficiency further by thickening the perovskite absorber layer (to >280 nm), replacing  $\text{MAPbI}_3$  with more stable CsFA mixed perovskites, replacing AZO with ITO to increase the thermal budget allowed during annealing, and replacing spin-coated electron/hole selective layers by vacuum-deposited counterparts without sacrificing the device performance.

Given that there were only seven perovskite–CIGS tandem demonstrations compared to 41 for perovskite–Si tandems, the pace of development for the former has been extraordinary [Fig. 7(b)]. Nevertheless, there is ample scope and motivation of further development due to the thin film advantages of perovskite–CIGS tandems, such as flexibility, solution processability, and bandgap tunability compared to the perovskite–Si tandem counterparts.

Moving forward, it is important to understand the challenges posed by the CIGS bottom cell. First, similar to the Si-heterojunction bottom cell with a TCO layer, the CIGS bottom cell can only withstand processing temperature below 200 °C. Second, the surface roughness of the CIGS cell is severe and irregular. Third, the polarity of CIGS cell limits the structure allowable for the perovskite cell. This means that developing a low-temperature processing for high-efficiency, high-bandgap p-i-n perovskite solar cells with conformal and full coverage on rough and irregular surfaces is critical to the success of perovskite–CIGS tandems.

Looking at the performance of the current state of the art perovskite–CIGS tandems,  $J_{SC}$  is still below 90% of the theoretical

**TABLE II.** Demonstrated monolithic perovskite–CIGS tandems.

Lower bandgap	Interface	Higher bandgap	V <sub>OC</sub> (V)	J <sub>SC</sub> (mA/cm <sup>2</sup> )	FF (%)	Eff. (%)	Area (cm <sup>2</sup> )	Reference
Glass/Si <sub>3</sub> N <sub>3</sub> /Mo/CIGS <sup>a</sup> /CdS (1.04 eV)	ITO	PEDOT:PSS/MAPbI <sub>X</sub> Br <sub>3-X</sub> /PCBM/Al (1.7 eV)	1.45	12.7	56.6	10.9	0.4	58
Glass/Mo/CIGS <sup>b</sup> /CdS/i-ZnO/BZO (1.1 eV)	ITO	PTAA/Cs <sub>0.09</sub> FA <sub>0.77</sub> MA <sub>0.14</sub> Pb(I <sub>0.86</sub> Br <sub>0.14</sub> ) <sub>3</sub> /PCBM/ZnO NPs/ITO (1.59 eV)	1.77	17.3	73.1	22.4 <sup>c</sup>	0.042	16
Glass/Mo/CIGSe <sup>d</sup> /i-ZnO (1.1 eV)	AZO	NiOx/PTAA/CsMAFAPbIBr/C60/SnO <sub>2</sub> /IZO (1.63 eV)	1.58	18.0	76.0	21.6	0.778	59
Polyimide substrate/Mo/CIGS <sup>d</sup> /CdS/i-ZnO (1.1 eV)	i-ZnO/AZO (ZnO:Al)	PTAA/CH <sub>3</sub> NH <sub>3</sub> PbI <sub>3</sub> /PCBM/ZnO NP/AZO/Ni-Al grid/MgF <sub>2</sub> (1.57 eV)	1.75	16.3	46.4	13.2	0.201	61
Glass/Mo/CIGSe <sup>d</sup> /i-ZnO (1.1 eV)	AZO	MeO-2PACz/Cs <sub>0.05</sub> (MA <sub>0.17</sub> FA <sub>0.83</sub> ) <sub>0.95</sub> Pb(I <sub>0.83</sub> B <sub>0.17</sub> ) <sub>3</sub> /C60/BCP/ITO/Cu or Ag grid/NaF (1.63 eV)	1.68	19.2	71.9	23.3 <sup>c</sup>	1.04	60
Glass/Mo/NaF/CIGS <sup>d</sup> /CdS/i-ZnO (1.1 eV)	AZO	NiO/FA <sub>0.83</sub> Cs <sub>0.17</sub> Pb(I <sub>0.83</sub> Br <sub>0.17</sub> ) <sub>3</sub> /LiF/PC <sub>60</sub> BM/SnO <sub>2</sub> /ITO/LiF (1.63 eV)	1.77	14.7	70.0	15.9	0.12	62
Glass/Mo/CIGSe <sup>d</sup> /i-ZnO (1.1 eV)	AZO	SAM/PEAI:Cs <sub>0.05</sub> (MA <sub>0.23</sub> FA <sub>0.77</sub> )Pb <sub>1.1</sub> (I <sub>0.77</sub> B <sub>0.23</sub> ) <sub>3</sub> /LiF/C60/SnO <sub>2</sub> /ITO/Cu or Ag grid/NaF (1.66 eV)	1.77	19.2	72.9	24.2 <sup>c</sup>	1.045	103

<sup>a</sup>Solution processed.<sup>b</sup>Sputtered.<sup>c</sup>Certified or independently verified.<sup>d</sup>Evaporation.<sup>e</sup>Steady-state.

limit, necessitating a thorough optical analysis of the state-of-the-art perovskite–CIGS tandem cells. This is to identify key optical losses and new cell designs for minimizing front reflection, Fresnel reflection, parasitic absorptions in interlayers and maximizing optical absorption by the CIGS and perovskite absorber layers. An approach that can improve the latter is by applying a back reflector, doubling the optical path length through the cells, which is present in Si solar cells and in single-junction perovskite solar cell. In terms of  $FF \times V_{OC}$ , the value is only 60% of its theoretical limit for perovskite–CIGS tandems compared to 70% for perovskite–Si tandems, necessitating improvements in cell design for better charge carrier management, such as the development of interface layer to enhance charge transport and surface passivation. There is also scope for further improving the performance of the CIGS cell, especially the quality of the rear surface passivation. Many of the CIGS cells used in tandem demonstrations have shown to have less than ideal external quantum efficiency (EQE) at long wavelength, e.g., at 1000 nm. This needs to be improved and is critically important as the CIGS cell will be solely responsible for long-wavelength absorption in a tandem.

### C. Perovskite–OPV tandem solar cells

Recently, there have been some interest in the demonstration of perovskite–OPV tandems (Fig. 9 and Table III) building on the advances in the improved stability and efficiency particularly from the recent emergence of non-fullerene acceptor for OPV.<sup>104,105</sup> OPV is also a solution processable technology and is advantageous when a non-polar solvent [e.g., chlorobenzene (CBZ)] is used for its fabrication, posing minimal damage to the perovskite cell which is fabricated first in a superstrate configuration. Therefore, the perovskite–OPV tandem is amenable to roll-to-roll manufacturing for flexible applications.<sup>84</sup> The first perovskite–OPV tandem demonstration was reported by Chen *et al.*<sup>82</sup> in 2015. While the order of the junctions is somewhat back-to-front with the lower-bandgap PBSeDTEG8:PCBM OPV cell being illuminated first followed by the higher-bandgap  $\text{CH}_3\text{NH}_3\text{PbI}_3$ , the team reported a 10.2% efficient tandem cell. Recent

demonstrations<sup>18,19</sup> have been successful in terms of boosting the efficiencies to above what can be achieved by OPV cell alone (>18.2%).<sup>7</sup>

However, the tandem efficiencies are still well below their theoretical limit (<50%) and lower than other perovskite tandem technologies [Fig. 3(c)]. This is because  $J_{SC}$  is below 80% of the theoretical limit. The tandem  $J_{SC}$  is limited by the bottom OPV cell as seen in the tandem external quantum efficiency curves.<sup>18,19</sup> Moving forward, an optical analysis identifying key optical losses for current and new cell designs will be useful. In terms of  $FF \times V_{OC}$ , the best value is around 60% of its theoretical limit. Again, this necessitates improvements in cell designs especially the interface layers which currently limit cell performance, as seen in the poorer EQE in the top cell near its absorption edge. Nevertheless, the pace of perovskite–OPV tandem development is extraordinary given that there have only been four demonstrations thus far, signaling ample scope and motivation of further development.

### D. Perovskite–perovskite tandem solar cells

The perovskite–perovskite tandem is a sensible pathway for low-cost, high-efficiency solar cells, as top and bottom cells share similar trajectories in terms of cell efficiency improvements, similar sensitivities to environmental stresses and therefore the same cell encapsulation and packaging requirements. The processing of top and bottom cells can also share similar infrastructure thereby lowering the capital expenditure. Figure 10 shows typical monolithic perovskite–perovskite tandem cell designs. Although both polarities have been demonstrated, the p-i-n cell structure is more favored.

The two most common challenges associated with the demonstration of 2-terminal perovskite–perovskite tandem is (i) the demonstration of high-efficiency low-bandgap typically Sn–Pb perovskite cells, and (ii) the development of interfacing between the top and bottom cell to minimize damage to the bottom cell during the processing of the top cell, to minimize the interface recombination and to maximize the carrier transport between the subcells.

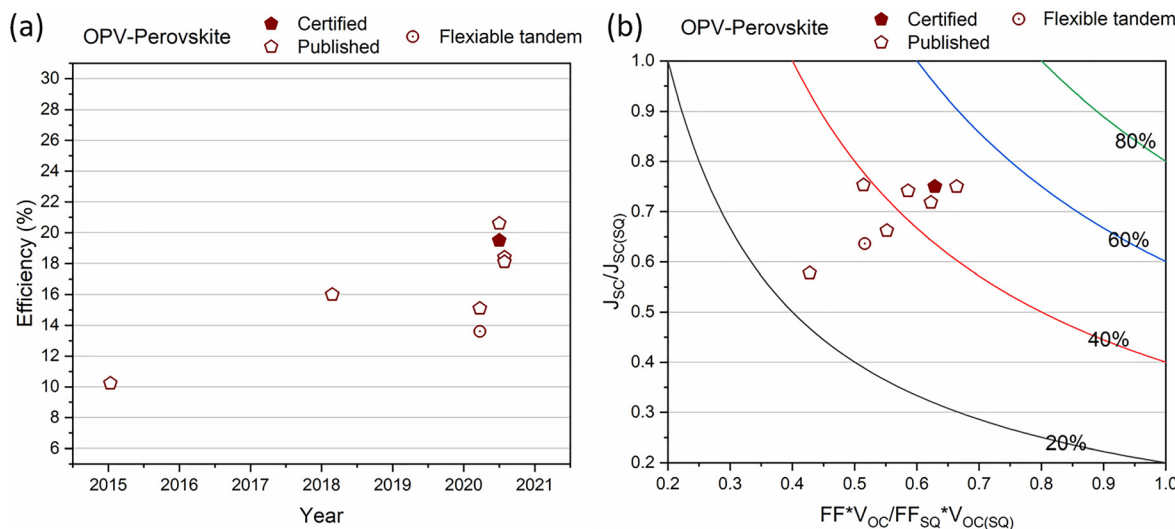


FIG. 9. Two terminal perovskite–OPV tandem solar cell: (a) evolution of energy conversion efficiency and (b)  $J_{SC}$  vs  $FF \times V_{OC}$  as a percentage of theoretical limits.

TABLE III. Demonstrated monolithic perovskite–OPV tandems.

Top cell	Interface	Bottom cell	$V_{OC}$ (V)	$J_{SC}$ (mA/cm <sup>2</sup> )	FF (%)	Eff. (%)	Area (cm <sup>2</sup> )	Reference
ITO/PEDOT:PSS/PBSeDTEG8: PCBM/PFN/TiO <sub>2</sub> (1.28 eV)	PEDOT:PSS PH500/ PEDOT:PSS4083	CH <sub>3</sub> NH <sub>3</sub> PbI <sub>3</sub> /PCBM/PFN/Al (1.51 eV)	1.52	10.1	67	10.2	0.1	82
ITO/PEDOT:PSS/CH <sub>3</sub> NH <sub>3</sub> PbI <sub>3</sub> / PC <sub>61</sub> BM (1.55 eV)	C <sub>60</sub> -SB/Ag/MoO <sub>3</sub>	PCE-10:PC <sub>71</sub> BM/C <sub>60</sub> -N/Ag (1.64 eV)	1.63	13.1	75	16.0	0.055	83
ITO/PTAA/CS <sub>0.1</sub> (FA <sub>0.6</sub> MA <sub>0.4</sub> ) <sub>0.9</sub> Pb(I <sub>0.6</sub> Br <sub>0.4</sub> ) <sub>3</sub> /PCBM/BCP (1.74 eV)	Ag	M-PEDOT/PBDB-T:SN6IC4F/Bis-C60/ BCP/Ag (1.30 eV)	1.85	11.5	71	15.1	0.13	84
ITO/NiOx/FA <sub>0.8</sub> MA <sub>0.2</sub> C <sub>60</sub> (1.77 eV)	BCP/Ag nanoparticle /MoO <sub>x</sub>	PBDBT-2F:Y6:PC <sub>71</sub> BM (1:1.2:0.2) (1.41 eV)	1.90	13.1	83	20.6	0.062	18
ITO/ZnO/SnO <sub>2</sub> /CsPbI <sub>2</sub> Br/ PDCBT (1.9 eV)	MoO <sub>3</sub> /Ag/ZnO	PM6:Y6-based/MoO <sub>3</sub> /Ag (1.37 eV) P'TPB7-Th:O6T-4F/MoO <sub>3</sub> /Ag (1.28 eV)	1.95	12.5	76	18.4	0.04	19

<sup>a</sup>Independently verified.

After the first “proof-of-concept” demonstrations using perovskites with non-ideal bandgaps, e.g., 1.5–1.5 (Ref. 64) and 2.25–1.5 eV,<sup>65</sup> a two-terminal perovskite–perovskite tandem using a low-bandgap (1.2 eV) Sn-containing perovskite for the bottom cell was demonstrated by Eperon *et al.*<sup>66</sup> in 2016. The champion cell achieved an efficiency of 17% and a  $V_{OC}$  of 1.66 V, which was higher than the  $V_{OC}$ 's of the individual cells. The key challenge associated with Sn-containing perovskite is its instability due to the tendency for Sn<sup>2+</sup> to oxidize into Sn<sup>4+</sup>.<sup>106</sup> Over the years, this has been overcome by incorporating SnF<sub>2</sub><sup>107</sup> or metallic Sn powders<sup>17</sup> in the perovskite precursor. Bulky organic cations, such as phenethylammonium (PEA)<sup>77</sup> or guanidinium (Gua),<sup>74</sup> have also been shown to be effective in reducing defects, thereby producing a high output voltage.

With regard to the fabrication method, physical deposition such as thermal evaporation has been explored to avoid the use of solution process which has the possibility of “dissolving” the bottom cell. Bolink and his colleagues<sup>67,70</sup> have championed this work for “n-i-p” perovskite–perovskite tandem. Starting with an ITO coated substrate, compact TiO<sub>2</sub> was deposited by solution processing as an electron transport layer (ETL) for the bottom cell. To reduce the recombination of the ETL/perovskite interface, fullerene derivative indene-C60-propionic acid hexyl ester (IPH) as an interlayer was deposited by solution processing. In their first work,<sup>67</sup> the bottom high-bandgap Cs<sub>0.15</sub>FA<sub>0.85</sub>Pb(I<sub>0.3</sub>Br<sub>0.7</sub>)<sub>3</sub> cell was fabricated by solution-processing while in their second work,<sup>67,70</sup> the bottom cell CH<sub>3</sub>NH<sub>3</sub>PbI<sub>3</sub> was fabricated by thermal evaporation, for the purpose of demonstrating all evaporated perovskite/perovskite tandem. Although the bandgap combination for the CH<sub>3</sub>NH<sub>3</sub>PbI<sub>3</sub>–CH<sub>3</sub>NH<sub>3</sub>PbI<sub>3</sub> tandem was non-ideal for best current output, the output voltage was one of the highest achieved for perovskite–perovskite tandems. For thermally evaporated electron transport layer, fullerene C<sub>60</sub> was used, which can be modulated by co-deposition of N1,N4-bis(tri-p-tolylphosphoranylidene)benzene-1,4-diamine (PhIm). For the hole transport material, N4,N4,N4'',N4''-tetra([1,1'-biphenyl]-4-yl)-[1,1':4',1''-terphenyl]-4,4''-diamine (TaTm) was evaporated and its conductivity can be tuned by doping it with 2,2'-(perfluoronaphthalene-2,6-diylidene) dimalononitrile (F6-TCNNQ) again via thermal evaporation. While physical-deposition is a promising approach for avoiding the use of solvent for the fabrication of perovskite–perovskite tandem, there remains scope for the demonstration of high-efficiency low-bandgap Sn–Pb perovskite cell by physical deposition.<sup>108,109</sup>

ITO or IZO was a popular choice for interfacing the top and bottom perovskite cells. For earlier demonstrations, their thickness were typically 100–130 nm, which was considered to be important for protecting the bottom cell from the solution processing of the top cell.<sup>66,68,69,73,74,76,78</sup> It was later found that a 5 nm ITO or IZO was sufficient for this purpose by Palmstrom *et al.*<sup>75</sup> They also reported that, for such thin transparent conductive layer to be effective, the depositions of a polyethylenimine (PEIE) layer by solution processing and an aluminum doped zinc oxide (AZO) layer by atomic layer deposition (ALD) were critical. The PEIE served as a nucleation layer for a dense and conformal AZO layer, which in turn allowed for a much thinner (5–10 nm) IZO to be deposited to form an efficient recombination junction.<sup>75</sup> However, more recent perovskite–perovskite tandem demonstrations no longer needed ITO or IZO, which was replaced by an ALD SnO<sub>x</sub> layer (9–20 nm) accompanied by 1 nm Au clusters to form a recombination junction.<sup>17</sup> This TCO-free design is suitable for large

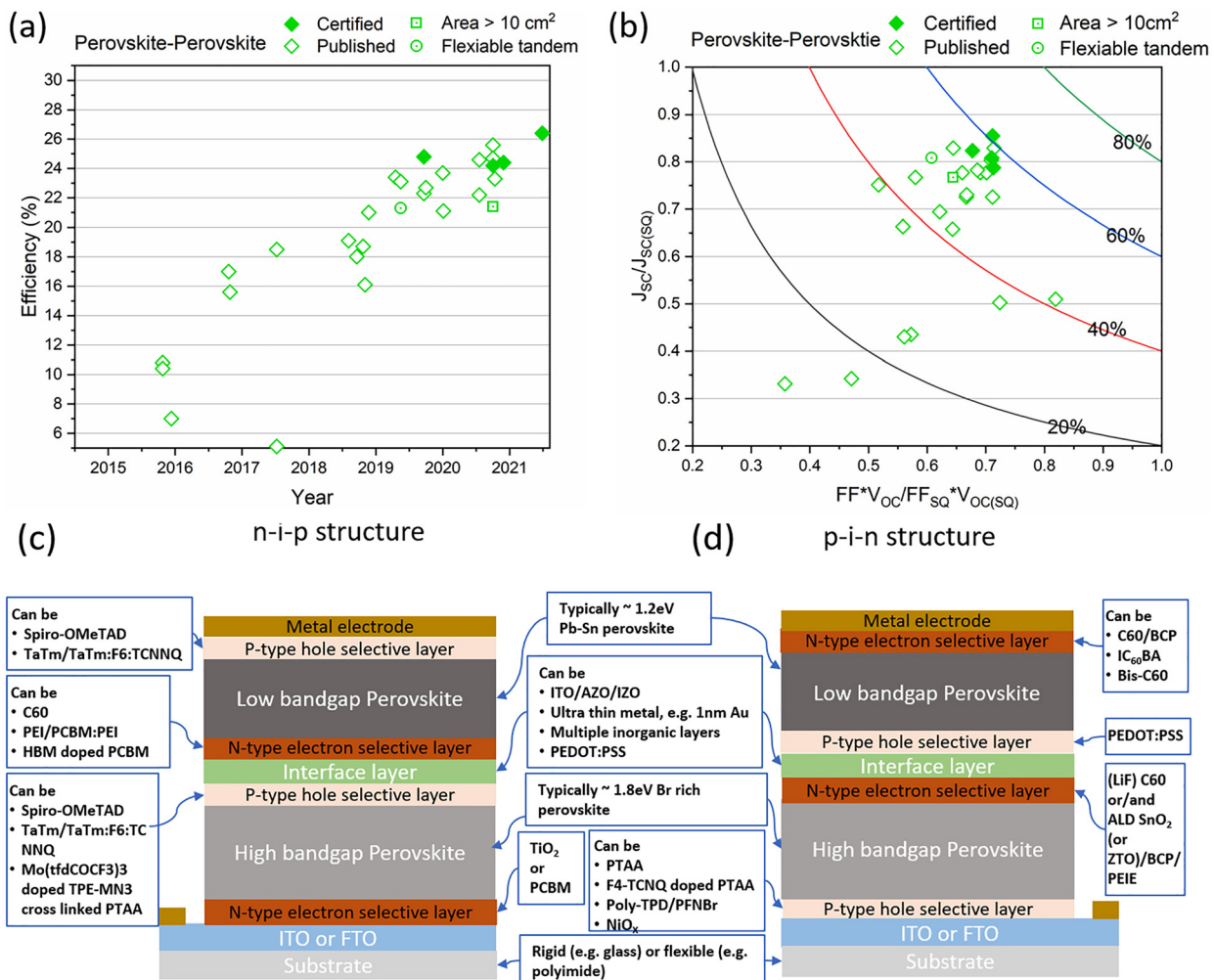


**FIG. 10.** Two terminal perovskite–perovskite tandem solar cell: (a) evolution of energy conversion efficiency, (b)  $J_{sc}$  vs  $FF \times V_{oc}$  as a percentage of theoretical limits, and (c) and (d) different types cell designs and associated challenges.

area tandems such as those demonstrated by Yu *et al.*<sup>79</sup> achieving 22.2% efficiency on  $1.15\text{ cm}^2$  area and by Xiao *et al.*<sup>80</sup> achieving a certified 24.2% efficiency on  $1\text{ cm}^2$  area and an efficiency of 21.4% on  $12\text{ cm}^2$  (first for perovskite–perovskite tandem  $>10\text{ cm}^2$ ). Most recently, the record efficiency of 26.4% on  $0.049\text{ cm}^2$  has been reported by the same group.<sup>100</sup> This is a milestone as the value exceeds the record efficiency of a single-junction perovskite solar cell.<sup>7</sup>

A problem faced by the current perovskite–perovskite tandems is the lower output current when compared with perovskite–Si tandems [Fig. 3(b)]. This is due to the thinness of the narrow bandgap perovskite layer in many of the demonstrated tandems ( $<$ ideal  $1100\text{--}1500\text{ nm}$ ). Fabricating a thick narrow bandgap Sn-containing perovskite film is not trivial due to its lower wettability and lower solubility compared to Pb perovskites. In 2018, Leijtens *et al.*<sup>69</sup> developed a route to fabricate uniform and thick ( $700\text{ nm}$ )  $\text{FA}_{0.75}\text{Cs}_{0.25}\text{Sn}_{0.5}\text{Pb}_{0.5}\text{I}_3$  by spin coating a high concentration ( $2.0\text{ M}$ ) of perovskite precursor solution followed by anisole antisolvent immersion treatment and a

methylammonium chloride (MACl) vapor accompanied by a short post-anneal at  $150^\circ\text{C}$ . While the fabrication of thick films was essential for improving light absorption and current output, the vapor treatment and the short post-anneal promoted grain size growth and the healing of cracks boosting fill factor and output voltage of the associated devices. These techniques of using high-concentration precursor<sup>81</sup> and Cl incorporation<sup>73</sup> have been shown to be effective by other researchers in fabricating thick ( $700\text{--}900\text{ nm}$ ) and high-quality tin-lead perovskites.

In 2019, Yang *et al.* reported that cadmium (Cd) incorporation (0.03%) reduces the trap density and improves the electron diffusion length of thick Sn–Pb perovskite.<sup>76</sup> Another use of Cd may be the doping ( $\leq 5\%$ ) of the Pb–Sn perovskite which, according to density functional theory (DFT) simulation,<sup>110</sup> can reduce its bandgap to  $1.1\text{ eV}$ , closer to the ideal bandgap— $0.96\text{ eV}$  for a bottom cell in a 2-junction tandem (Fig. 2). However, there is still a large disparity between the theoretical limit and the actual output voltage resulting in a voltage

**TABLE IV.** Demonstrated monolithic perovskite–perovskite tandems. FSIP = Fluoride silane-incorporated polyethylenimine ethoxylated hybrid system.

Higher-bandgap bottom cell	Interface	Lower-bandgap top cell	V <sub>OC</sub> (V)	J <sub>SC</sub> (mA/cm <sup>2</sup> )	FF (%)	Eff. (%)	Area (cm <sup>2</sup> )	Reference
Glass/FTO/c-TiO <sub>2</sub> /m-TiO <sub>2</sub> /MAPbI <sub>3</sub> /spiro-OMeTAD (1.55 eV)	PEDOT:PSS	PEI/PCBM:PEI/MAPbI <sub>3</sub> /spiro-OMeTAD/Ag (1.55 eV)	1.89	6.61	56	7.0	0.1	64
Glass/FTO/bl-TiO <sub>2</sub> /MAPbBr <sub>3</sub> (2.25 eV)	wet P3HT wet PTAA	PCBM/MAPbI <sub>3</sub> /PEDOT:PSS/ITO/Glass (1.55 eV)	1.95	8.4	66	10.8	0.096	65
	ITO		2.25	8.3	56	10.4	0.096	
Glass/ITO/NiO/FA <sub>0.83</sub> Cs <sub>0.17</sub> Pb(I <sub>0.5</sub> Br <sub>0.5</sub> ) <sub>3</sub> /PCBM/SnO <sub>2</sub> /ZTO (1.8 eV)	ITO	PEDOT:PSS/FA <sub>0.75</sub> Cs <sub>0.25</sub> Sn <sub>0.5</sub> Pb <sub>0.5</sub> I <sub>3</sub> /C <sub>60</sub> /BCP/Ag (1.2 eV)	1.66	14.5	70	17.0	0.2	66
Glass/ITO/TiO <sub>2</sub> /IPH/Cs <sub>0.15</sub> FA <sub>0.85</sub> Pb(I <sub>0.3</sub> Br <sub>0.7</sub> ) <sub>3</sub> /TaTm/TaTm:F6:TCNNQ/Au (2.0 eV)	C <sub>60</sub> :PhIm	C <sub>60</sub> /MAPbI <sub>3</sub> /TaTm/TaTm:F6:TCNNQ/Au (1.55 eV)	2.14	9.7	76	15.6	0.026	67
Glass/ITO/NiOx/MA <sub>0.9</sub> Cs <sub>0.1</sub> Pb(I <sub>0.6</sub> Br <sub>0.4</sub> ) <sub>3</sub> /C <sub>60</sub> /Bis-C <sub>60</sub> (1.82 eV)	ITO	PEDOT:PSS/MAPb <sub>0.5</sub> Sn <sub>0.5</sub> I <sub>3</sub> /IC <sub>60</sub> BA/Bis-C <sub>60</sub> /Ag (1.22 eV)	1.98	12.7	73	18.5	0.1	68
Glass/FTO/c-TiO <sub>2</sub> /m-TiO <sub>2</sub> /MAPbBr <sub>3</sub> /spiro-OMeTAD (2.25 eV)	PEDOT:PSS	C <sub>60</sub> /MAPbI <sub>3</sub> /spiro-OMeTAD/Au (1.55 eV)	1.96	6.4	41	5.1	0.16	111
Glass/ITO/PTAA/FA <sub>0.6</sub> Cs <sub>0.4</sub> Pb(I <sub>0.7</sub> Br <sub>0.3</sub> ) <sub>3</sub> /C <sub>60</sub> /ZTO (1.76 eV)	ITO	PEDOT:PSS/FA <sub>0.75</sub> Cs <sub>0.25</sub> Sn <sub>0.5</sub> Pb <sub>0.5</sub> I <sub>3</sub> /C <sub>60</sub> /BCP/Ag (1.25 eV)	1.81	14.8	72	19.1	...	69
Glass/ITO/TiO <sub>2</sub> /C <sub>60</sub> /MAPbI <sub>3</sub> /TaTm/TaTm:F6:TCNNQ (1.55 eV)	C <sub>60</sub> :PhIm	C <sub>60</sub> /MAPbI <sub>3</sub> /TaTm/TaTm:F6:TCNNQ/Au (1.55 eV)	2.30	9.84	80	18.0	0.12	70
Glass/ITO/NiO <sub>x</sub> /FA <sub>0.83</sub> Cs <sub>0.17</sub> Pb(Br <sub>0.5</sub> I <sub>0.5</sub> ) <sub>3</sub> /FSIP/C <sub>60</sub> /BCP (1.83 eV)	Cu/Au	PEDOT:PSS/FA <sub>0.5</sub> MA <sub>0.5</sub> Pb <sub>0.5</sub> Sn <sub>0.5</sub> I <sub>3</sub> /polystyrene/C <sub>60</sub> /BCP/Ag (1.24 eV)	1.72	12.8	73	16.1	0.034	71
Glass/ITO/TiO <sub>x</sub> /PC <sub>61</sub> BM/MAPbI <sub>3</sub> /Mo(tfdCOCF <sub>3</sub> ) <sub>3</sub> doped TPE-MN3 cross-linked PTAA/ (1.55 eV)		HMB-doped PC <sub>61</sub> BM/MASn <sub>0.25</sub> Pb <sub>0.75</sub> I <sub>3</sub> /Spiro-OMeTAD/Ag (1.25 eV)	1.79	13.4	78	18.7	0.12	72
Glass/ITO/F <sub>4</sub> -TCNNQ doped PTAA/FA <sub>0.8</sub> Cs <sub>0.2</sub> Pb(I <sub>0.7</sub> Br <sub>0.3</sub> ) <sub>3</sub> /C <sub>60</sub> /BCP (1.75 eV)	Ag/MoO <sub>x</sub> /ITO	PEDOT:PSS/(FASnI <sub>3</sub> ) <sub>0.6</sub> (MAPbI <sub>3</sub> ) <sub>0.4</sub> :Cl/ C <sub>60</sub> /BCP/Ag (1.26 eV)	1.92	14.0	78	21.0	0.105	73
Glass/ITO/PTAA/CS <sub>0.05</sub> FA <sub>0.8</sub> MA <sub>0.15</sub> PbI <sub>2.55</sub> Br <sub>0.45</sub> /C <sub>60</sub> /SnO <sub>x</sub> /ZTO (1.75 eV)	IZO	PEDOT:PSS/GuaSCN:(FASnI <sub>3</sub> ) <sub>0.6</sub> (MAPbI <sub>3</sub> ) <sub>0.4</sub> /C <sub>60</sub> /BCP/Ag (1.25 eV)	1.94	15.0	80	23.4	0.059	74
Glass/ITO/PolyTPD/PFN-Br/FA <sub>0.6</sub> Cs <sub>0.3</sub> DMA <sub>0.1</sub> PbI <sub>2.4</sub> Br <sub>0.6</sub> /LiF/C <sub>60</sub> /PEIE (1.70 eV)	AZO/IZO	PEDOT:PSS/FA <sub>0.75</sub> Cs <sub>0.25</sub> Sn <sub>0.5</sub> Pb <sub>0.5</sub> I <sub>3</sub> /C <sub>60</sub> /BCP/Ag (1.27 eV)	1.88	16.0	77	23.1	0.058	75
			1.82	15.6	75	21.3	0.058	
Glass/ITO/PTAA/FA <sub>0.8</sub> Cs <sub>0.2</sub> Pb(I <sub>0.6</sub> Br <sub>0.4</sub> ) <sub>3</sub> /C <sub>60</sub> (1.77 eV)	SnO <sub>2</sub> /Au	PEDOT:PSS/PTAA/ Cd:FA <sub>0.5</sub> MA <sub>0.45</sub> Cs <sub>0.05</sub> Sn <sub>0.5</sub> Pb <sub>0.5</sub> I <sub>3</sub> /C <sub>60</sub> /BCP/Cu (1.22 eV)	1.93	15.8	81	24.8 <sup>a</sup>	0.048	17
Glass/ITO/PTAA/FA <sub>0.6</sub> Cs <sub>0.4</sub> Pb(I <sub>0.65</sub> Br <sub>0.35</sub> ) <sub>3</sub> /C <sub>60</sub> /SnO <sub>2</sub> (1.80 eV)	ITO	PEDOT:PSS/PTAA/ Cd:FA <sub>0.5</sub> MA <sub>0.45</sub> Cs <sub>0.05</sub> Sn <sub>0.5</sub> Pb <sub>0.5</sub> I <sub>3</sub> /C <sub>60</sub> /BCP/Cu (1.22 eV)	1.95	15.0	76	22.7	0.068	76

TABLE IV. (Continued.)

Higher-bandgap bottom cell	Interface	Lower-bandgap top cell	$V_{OC}$ (V)	$J_{SC}$ (mA/cm <sup>2</sup> )	FF (%)	Eff. (%)	Area (cm <sup>2</sup> )	Reference
Glass/ITO/PTAA/FA <sub>0.8</sub> Cs <sub>0.2</sub> PbI <sub>1.8</sub> Br <sub>1.2</sub> /C <sub>60</sub> (1.77 eV)	SnO <sub>2</sub> /Au	PEDOT:PSS/PEAI:Cs <sub>0.1</sub> MA <sub>0.2</sub> FA <sub>0.7</sub> Pb <sub>0.5</sub> Sn <sub>0.5</sub> I <sub>3</sub> /C <sub>60</sub> /BCP/Ag (1.25 eV)	1.97	15.0	80	23.7	0.049	77
Glass/ITO/PTAA/FA <sub>0.8</sub> Cs <sub>0.2</sub> Pb(I <sub>0.7</sub> Br <sub>0.3</sub> ) <sub>3</sub> /C <sub>60</sub> /BCP (1.75 eV)	ITO	PEDOT:PSS/(FASnI <sub>3</sub> ) <sub>0.6</sub> (MAPbI <sub>3</sub> ) <sub>0.4</sub> /C <sub>60</sub> /BCP/Ag (1.25 eV)	1.91	14.1	79	21.1	0.12	78
Glass/ITO/NiO/VNPB/FA <sub>0.8</sub> Cs <sub>0.2</sub> Pb(I <sub>0.6</sub> Br <sub>0.4</sub> ) <sub>3</sub> /C <sub>60</sub> (1.77 eV)	SnO <sub>2</sub> /Au	PEDOT:PSS/FSA:MA <sub>0.3</sub> FA <sub>0.7</sub> Pb <sub>0.5</sub> Sn <sub>0.5</sub> I <sub>3</sub> /C <sub>60</sub> /BCP/Cu (1.22 eV)	2.01	16.0	80	25.6	0.049	80
			1.99	15.9	77	24.2 <sup>a</sup>	1.04	
			1.96	14.8	74	21.4	12	
Glass/ITO/PTAA/Cs <sub>0.4</sub> FA <sub>0.6</sub> PbI <sub>1.95</sub> Br <sub>1.05</sub> (1.78 eV)	C <sub>60</sub> /SnO <sub>1.76</sub>	Cs <sub>0.05</sub> MA <sub>0.45</sub> FA <sub>0.5</sub> Pb <sub>0.5</sub> Sn <sub>0.5</sub> I <sub>3</sub> /C <sub>60</sub> /BCP/Cu (1.25 eV)	2.03	15.2	80	24.6	0.059	79
			2.01	15.5	79	22.2	1.05	
Glass/ITO/PTAA/FA0.85MA0.1Cs0.05Sn0.5Pb0.5I3/C60 /BCP (1.73 eV)	ITO	PEDOT:PSS/(FASnI3)0.6(MAPbI3)0.4 /C60/BCP/Cu (1.28 eV)	1.94	15.1	79	23.3	0.12	81
?	?	?	2.00	15.2	80	24.4 <sup>a</sup>	0.049	89
?	?	?	2.05	16.5	78	26.4 <sup>a</sup>	0.049	100

<sup>a</sup>Certified or independently verified.<sup>b</sup>Steady-state.

TABLE V. Demonstrated 3-junction monolithic perovskite tandems.

Higher bandgap	Interface	Middle bandgap	Interface	Lower bandgap	$V_{OC}$ (V)	$J_{SC}$ (mA/cm <sup>2</sup> )	FF (%)	Eff. (%)	Area (cm <sup>2</sup> )	Reference
Glass/FTO/SnO <sub>2</sub> /FA <sub>0.83</sub> Cs <sub>0.17</sub> Pb(Br <sub>0.7</sub> I <sub>0.3</sub> ) <sub>3</sub> /Spiro-OMeTAD (1.94 eV)	PEDOT:PSS/ITO NPs	PC <sub>61</sub> BM/MAPbI <sub>3</sub> /Spiro-OMeTAD (1.57 eV)	PEDOT:PSS/ITO NPs	PC <sub>61</sub> BM/MAPb <sub>0.75</sub> Sn <sub>0.25</sub> I <sub>3</sub> /Spiro-(TFSI) <sub>2</sub> /Ag (1.34 eV)	2.7	8.3	43	6.7	0.0919	112
Glass/ITO/PTAA/Cs <sub>0.2</sub> FA <sub>0.8</sub> PbI <sub>0.9</sub> Br <sub>2.1</sub> /C <sub>60</sub> (1.99 eV)	ALD-SnO <sub>2</sub> /Au	NiO/PTAA/Cs <sub>0.05</sub> FA <sub>0.95</sub> PbI <sub>2.55</sub> Br <sub>0.45</sub> /C <sub>60</sub> (1.60 eV)	ALD-SnO <sub>2</sub> /Au	PEDOT:PSS/MA <sub>0.3</sub> FA <sub>0.7</sub> Pb <sub>0.5</sub> Sn <sub>0.5</sub> I <sub>3</sub> /C <sub>60</sub> /BCP/Cu (1.22 eV)	2.80	8.8	81	20.1	0.049	113
Glass/ITO/PTAA/Cs <sub>0.1</sub> (FA <sub>0.66</sub> MA <sub>0.34</sub> ) <sub>0.9</sub> PbI <sub>2</sub> Br/C <sub>60</sub> (1.73 eV)	ALD-SnO <sub>2</sub> /Au	PEDOT:PSS/PTAA/FA <sub>0.66</sub> MA <sub>0.34</sub> PbI <sub>2.85</sub> Br <sub>0.15</sub> /C <sub>60</sub> (1.57 eV)	ALD-SnO <sub>2</sub> /Au	FA <sub>0.66</sub> MA <sub>0.34</sub> Pb <sub>0.5</sub> Sn <sub>0.5</sub> I <sub>3</sub> /C <sub>60</sub> /BCP/Ag (1.23 eV)	2.78	7.4	81	16.8	0.0667	114
MgF <sub>2</sub> /IZO/SnO <sub>2</sub> /C <sub>60</sub> /LiF/CsFAPbIBr/CsFAPbIBr/NiO (1.8 eV)	IZO	SnO <sub>2</sub> /C <sub>60</sub> /LiF/CsFAPbIBr/spiro-TTB (1.53 eV)	nc-Si:H(p+)/nc-Si:H(n+)	SHJ [a-Si(n) front/n-Si] (1.1 eV)	2.69	7.7	68	14.0	1.42	115

deficit ( $W_{OC} = Eg/q - V_{OC}$ ) from Pb–Sn perovskites, larger than that of Pb-only perovskites. This is due to the low external radiative efficiency (ERE).<sup>14</sup> This means there is no incentive to reduce the bandgap of the lower-bandgap-cell until the quality of the absorber layer is greatly improved. This means, in the short term, the bandgap of the bottom cell can be higher than ideal in order to deliver the required output voltage<sup>14</sup> for tandems.

### E. Triple-junction tandem

A 3-junction perovskite–perovskite–perovskite tandem will lower the burden placed on the bottom cell as mid- to low-energy incident photons will be distributed between the middle and bottom cells. As efficiencies of 2-junction tandems reach 30%, the rate of improvement may stagnate. Triple-junction concept provides an opportunity for an efficiency leap.<sup>116,117</sup> While the theoretical efficiency for a triple-junction tandem is 51%,<sup>6</sup> Horantner *et al.*<sup>118</sup> reported that the practical efficiency

limits for triple-junction perovskite–perovskite–perovskite cell would be 36.6% (with a bandgap combination of 2.04, 1.58, and 1.22 eV for the top, middle, and bottom cell, respectively) and for triple-junction perovskite–perovskite–Si cell would be 38.8% (for a combination of 1.95, 1.44, and 1.1 eV) as shown in Fig. 11.

To date, there are three demonstrations of all perovskite triple-junction tandems<sup>112–114</sup> and one on perovskite–perovskite–Si tandem.<sup>115</sup> All these produced  $V_{OC} \geq 2.7$  V. The best triple junction tandems<sup>113,114</sup> produced  $FF \times V_{OC}$  products that are 73% of the practical limits reported in Ref. 118, suggesting a reasonable quality of interfacing between the cells in these perovskite–perovskite–perovskite tandems.<sup>113,114</sup> There is a large scope for improvement in terms of current outputs which are well below the practical limits<sup>118</sup> (only 55% for demonstrated perovskite–perovskite–Si tandems to 68% for demonstrated perovskite–perovskite–perovskite tandems). This is due to the large mismatch between the subcells as seen by their external quantum efficiencies (EQE).<sup>112–114</sup> In these works, it is often the case that one

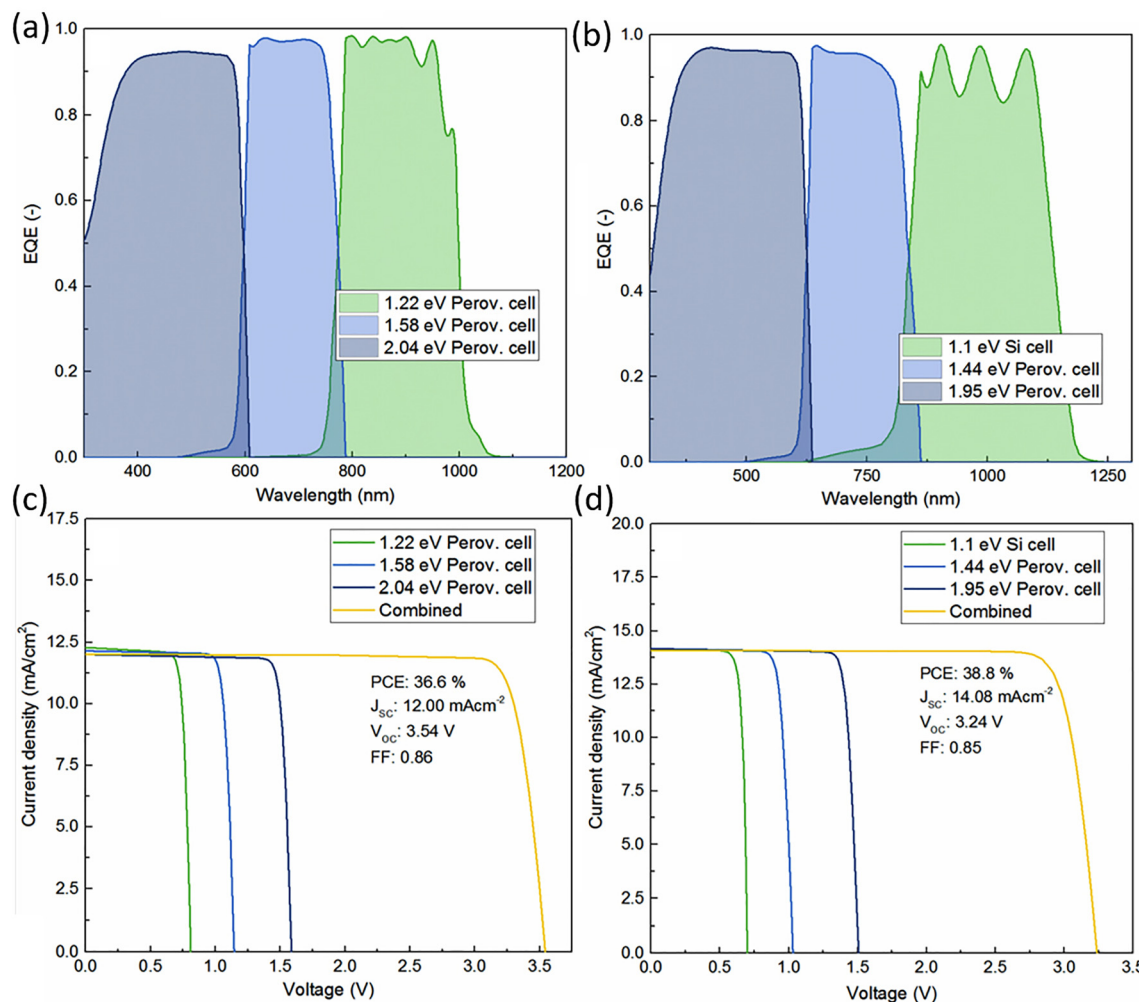


**FIG. 11.** Practical limits for triple junction. Simulated external quantum efficiencies and current–density voltage curves for ideal (a) and (c) perovskite–perovskite–perovskite and (b) and (d) perovskite–perovskite–Si tandems.<sup>118</sup> Reproduced with permission from Hörantner *et al.*, ACS Energy Lett. 2, 2506 (2017). Copyright 2017 American Chemical Society.

subcell has an EQE of  $<60\%$ , thereby limiting the output of the overall tandem, while subcells are connected in series sharing the same low current output. This shows the importance of good cell designs that minimize optical losses such as front reflection, Fresnel reflection, and parasitic absorptions in interlayers. However, the task is non-trivial as each additional subcell typically introduces three to four additional interlayers, contributing to optical losses and fabrication complexity.

## F. Future prospects for perovskite tandem solar cells

To truly realize the full potentials of double- and triple-junction tandems that have theoretical power conversion efficiency of 45% and 51%, respectively, it is important that wide-bandgap cells deliver their potential output voltage, which multi-junction tandems rely on for achieving high efficiencies.<sup>119,120</sup>

Figure 12 shows that while some perovskite cells with bandgap ( $E_g \leq 1.8$  eV) have been able to produce  $V_{OC} \sim 90\%$  of their

theoretical limits<sup>29,34,36,42,49,52–54</sup>—relevant to double-junction tandems,<sup>56</sup> cells with  $E_g > 1.8$  eV (relevant to triple-junction tandems) have not been able to do so.<sup>121</sup> This is due to the halide segregation that commonly occurs<sup>120</sup> in the mixed Br-I perovskites with bandgaps  $<2.3$  eV. Although high voltages can be achieved by tribromide perovskites (without the halide segregation), their bandgaps ( $\sim 2.3$  eV) are too high for most multi-junction cells.<sup>6</sup> Therefore, strategies for understanding<sup>121</sup> and suppressing halide segregation (turning to inorganic cations<sup>122</sup> to reduce the reliance on Br for tuning bandgap, for example) and strategies for maximizing voltage output from high-bandgap perovskite solar cells are critical for the success of perovskite tandem solar cells.

Common strategies for maximizing voltages of small bandgap cells include compositional engineering<sup>29,42</sup> additive engineering<sup>36,53,74,76</sup> surface or bulk passivation<sup>51,73,80,123</sup> can be translated to wide-bandgap cells [e.g., the use of  $Pb(SCN)_2$ <sup>124</sup> and formamidinium acetate<sup>123</sup>]. Two-dimensional (2D) perovskite layer for surface

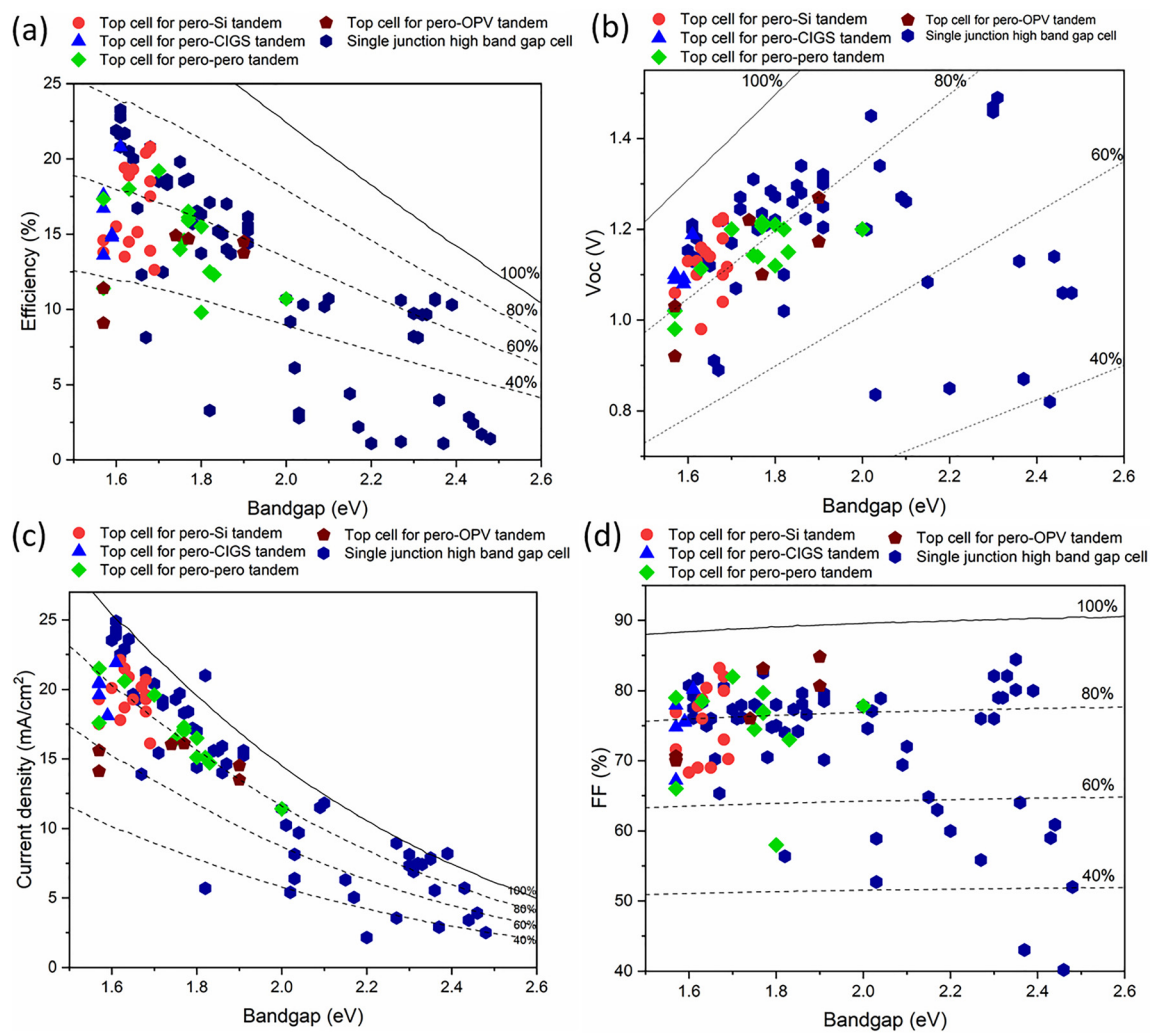


FIG. 12. Reported photovoltaic parameters of perovskite solar cells of various bandgaps. The dashed lines indicate the proportions of the SQ limits.<sup>9,124–130,132–171</sup>

passivation employing n-butylammonium bromide,<sup>9,125</sup> bilateral alkylamine additive, 1,3-diaminopropane,<sup>126</sup> and iso-butylammonium<sup>127</sup> have been reported to be effective. Doping or incorporation by Ba ions,<sup>128</sup> Eu ions,<sup>129</sup> Europium ion pair Eu<sup>3+</sup>-Eu<sup>2+</sup><sup>130</sup> and K ions<sup>131</sup> have been reported to improve the quality of wide-bandgap perovskites. Apart from improving perovskite bulk quality and surface (including double sided passivations<sup>132</sup>) appropriate choice of carrier selective layers is also important.<sup>60,73</sup> Not only can these provide additional passivation [e.g., in zwitterion-modified SnO<sub>2</sub> electron transport layer (ETL)<sup>133</sup>] and achieve desirable work function (e.g., NH<sub>4</sub>Cl modification of ZnO ETL<sup>134</sup> and self-assembled monolayer (SAM) with methyl group substitution Me-4PACz {[4-(3,6-dimethyl-9H-carbazol-9-yl)butyl] phosphonic acid} for hole transport layer (HTL)<sup>15</sup>] to facilitate better carrier transport, but also they can influence the quality of the perovskite film subsequently deposited.<sup>134</sup> Recently, LiF has become a popular interlayer as part of the ETL stack modification layer for high-efficiency high-bandgap perovskite cells<sup>31,44,51,52,85</sup> in demonstrated tandems.

Regarding scale-up to large-area cell fabrication, learnings from the recently increasing effort in large-area single-junction cell demonstrations<sup>172</sup> will be translated to tandems. However, the purpose or focus for flexible thin film tandems are different to those for perovskite–Si tandem. Perovskite–Si tandem deals with a flat, rigid substrate with a well-defined area. Perovskite–CIGS, perovskite–OPV, and perovskite–perovskite tandems on the other hand involve larger area deposition and require sectioning of the cells into strips followed by re-connection. The deposition methods also extend to roll-to-roll printing capitalizing on the flexible nature of thin film technologies. While there is a large scope of work, progress in large area perovskite-based thin film tandems will be at a slower pace compared to perovskite–Si tandems.

In terms of durability requirements, the expectation for perovskite–Si tandem will be higher as it is seen as a technology that will boost the performance of the incumbent. This is because, for tandems to be cost-effective, not only must the increase in cost in \$/cell (due to the additional cost of fabricating the top perovskite cell) be matched by an increase in efficiency, but also the lifetime of the perovskite sub cell must match that of the Si solar cell.<sup>90</sup> This may mean a 15-year-product warranty and 14% degradation performance warranty of 25 years allowing for 2% degradation in the 1st year followed by 0.5% degradation each successive year.<sup>1</sup> For thin film perovskite tandems such as perovskite–CIGS, perovskite–OPV, and perovskite–perovskite tandems, while the expectations will be lower due to the lower technology readiness levels, the challenge will be no less due to the current reliance on Sn–Pb mixed perovskite for the bottom narrow bandgap cell, with Sn having a tendency to oxidize from Sn<sup>2+</sup> to Sn<sup>4+</sup> and the problem of halide segregation in high-bandgap mixed halide perovskites. Some of these issues may be overcome by the recently emerged two-dimensional (2D) metal halide perovskites,<sup>9,77,125,127,132,167</sup> which have become a new favorite (evident by the increasing number of papers in recent years) because of the expanded range of material properties allowable improving their functionality and stability compared to 3D metal halide perovskites.

### III. CONCLUSION AND OUTLOOK

While some of the issues are unique to each technology, common challenges include the development of high-performance and stable

wide-bandgap perovskite, which is most critical for the full potential of perovskite-multi-junction cells to be realized. It is believed that with the sustained research and development (R&D) followings of perovskite photovoltaics, continued progress will be made and breakthroughs in triple-junction tandems will be reported in the very near future.

### AUTHORS' CONTRIBUTIONS

A.W.Y.H.-B. and J.Z. contributed equally to this work.

### ACKNOWLEDGMENTS

This work was supported by the Australian Government through the Australian Renewable Energy Agency (ARENA) via Project Nos. 2020 RND001 and 2020 RND003 and the Australian Centre for Advanced Photovoltaics (ACAP) Postdoctoral Fellowships.

There are no conflicts to declare.

### DATA AVAILABILITY

The data that support the findings of this study are available from the corresponding author upon reasonable request.

The data that support the findings in others' publications and are presented in this review are available from the corresponding authors of publications cited in this review. Restrictions may apply to the availability of these data.

### REFERENCES

- <sup>1</sup>The Mechanical Engineering Industry Association for PV (VDMAPV), *International Technology Roadmap for Photovoltaic (ITRPV). 2019 Results*, 11th ed. (Mechanical Engineering Industry Association for PV, 2020).
- <sup>2</sup>P. K. Nayak, S. Mahesh, H. J. Snaith, and D. Cahen, "Photovoltaic solar cell technologies: Analysing the state of the art," *Nat. Rev. Mater.* **4**(4), 269–285 (2019).
- <sup>3</sup>R. M. Swanson, "Approaching the 29% limit efficiency of silicon solar cells," in *Conference Record of the Thirty-First IEEE Photovoltaic Specialists Conference* (IEEE, 2005), pp. 889–894.
- <sup>4</sup>A. Richter, M. Hermle, and S. W. Glunz, "Reassessment of the limiting efficiency for crystalline silicon solar cells," *IEEE J. Photovoltaics* **3**(4), 1184–1191 (2013).
- <sup>5</sup>M. A. Green, "Limiting photovoltaic efficiency under new ASTM International G173-based reference spectra," *Prog. Photovoltaics* **20**(8), 954–959 (2012).
- <sup>6</sup>S. P. Bremner, C. Yi, I. Almansouri, A. Ho-Baillie, and M. A. Green, "Optimum band gap combinations to make best use of new photovoltaic materials," *Sol. Energy* **135**, 750–757 (2016).
- <sup>7</sup>See <https://www.nrel.gov/pv/cell-efficiency.html> for NREL (last accessed Aug 19, 2021).
- <sup>8</sup>L. C. Hirst and N. Ekins-Daukes, "Fundamental losses in solar cells," *Prog. Photovoltaics* **19**(3), 286–293 (2011).
- <sup>9</sup>T. Duong, H. Pham, T. C. Kho, P. Phang, K. C. Fong, D. Yan, Y. Yin, J. Peng, M. A. Mahmud, S. Gharibzadeh, B. A. Nejand, I. M. Hossain, M. R. Khan, N. Mozaffari, Y. Wu, H. Shen, J. Zheng, H. Mai, W. Liang, C. Samundsett, M. Stocks, K. McIntosh, G. G. Andersson, U. Lemmer, B. S. Richards, U. W. Paetzold, A. Ho-Baillie, Y. Liu, D. Macdonald, A. Blakers, J. Wong-Leung, T. White, K. Weber, and K. Catchpole, "High efficiency perovskite–silicon tandem solar cells: Effect of surface coating versus bulk incorporation of 2D perovskite," *Adv. Energy Mater.* **10**, 1903553 (2020).
- <sup>10</sup>Y. Ko, H. Park, C. Lee, Y. Kang, and Y. Jun, "Recent progress in interconnection layer for hybrid photovoltaic tandems," *Adv. Mater.* **32**(51), 2002196 (2020).

- <sup>11</sup>Z. Zhu, K. Mao, and J. Xu, "Perovskite tandem solar cells with improved efficiency and stability," *J. Energy Chem.* **58**, 219–232 (2021).
- <sup>12</sup>M. A. Green, A. Ho-Baillie, and H. J. Snaith, "The emergence of perovskite solar cells," *Nat. Photonics* **8**(7), 506–514 (2014).
- <sup>13</sup>A. Kojima, K. Teshima, Y. Shirai, and T. Miyasaka, "Organometal halide perovskites as visible-light sensitizers for photovoltaic cells," *J. Am. Chem. Soc.* **131**(17), 6050–6051 (2009).
- <sup>14</sup>M. A. Green and A. W. Y. Ho-Baillie, "Pushing to the limit: Radiative efficiencies of recent mainstream and emerging solar cells," *ACS Energy Lett.* **4**(7), 1639–1644 (2019).
- <sup>15</sup>A. Al-Ashouri, E. Köhnen, B. Li, A. Magomedov, H. Hempel, P. Caprioglio, J. A. Márquez, A. B. M. Vilches, E. Kasparavicius, and J. A. Smith, "Monolithic perovskite/silicon tandem solar cell with >29% efficiency by enhanced hole extraction," *Science* **370**(6522), 1300–1309 (2020).
- <sup>16</sup>Q. Han, Y.-T. Hsieh, L. Meng, J.-L. Wu, P. Sun, E.-P. Yao, S.-Y. Chang, S.-H. Bae, T. Kato, V. Bermudez, and Y. Yang, "High-performance perovskite/Cu(In,Ga)Se<sub>2</sub> monolithic tandem solar cells," *Science* **361**(6405), 904–908 (2018).
- <sup>17</sup>R. Lin, K. Xiao, Z. Qin, Q. Han, C. Zhang, M. Wei, M. I. Saidaminov, Y. Gao, J. Xu, M. Xiao, A. Li, J. Zhu, E. H. Sargent, and H. Tan, "Monolithic all-perovskite tandem solar cells with 24.8% efficiency exploiting comproportionation to suppress Sn(II) oxidation in precursor ink," *Nat. Energy* **4**(10), 864–873 (2019).
- <sup>18</sup>X. Chen, Z. Jia, Z. Chen, T. Jiang, L. Bai, F. Tao, J. Chen, X. Chen, T. Liu, X. Xu, C. Yang, W. Shen, W. E. I. Sha, H. Zhu, and Y. Yang, "Efficient and reproducible monolithic perovskite/organic tandem solar cells with low-loss interconnecting layers," *Joule* **4**(7), 1594–1606 (2020).
- <sup>19</sup>S. Xie, R. Xia, Z. Chen, J. Tian, L. Yan, M. Ren, Z. Li, G. Zhang, Q. Xue, H.-L. Yip, and Y. Cao, "Efficient monolithic perovskite/organic tandem solar cells and their efficiency potential," *Nano Energy* **78**, 105238 (2020).
- <sup>20</sup>K. Yoshikawa, H. Kawasaki, W. Yoshida, T. Irie, K. Konishi, K. Nakano, T. Uto, D. Adachi, M. Kanematsu, and H. Uzu, "Silicon heterojunction solar cell with interdigitated back contacts for a photoconversion efficiency over 26%," *Nat. Energy* **2**(5), 17032 (2017).
- <sup>21</sup>M. Nakamura, K. Yamaguchi, Y. Kimoto, Y. Yasaki, T. Kato, and H. Sugimoto, "Cd-free Cu (In, Ga)(Se, S)<sub>2</sub> thin-film solar cell with record efficiency of 23.35%," *IEEE J. Photovoltaics* **9**(6), 1863–1867 (2019).
- <sup>22</sup>J. P. Mailoa, C. D. Bailie, E. C. Johlin, E. T. Hoke, A. J. Akey, W. H. Nguyen, M. D. McGehee, and T. Buonassisi, "A 2-terminal perovskite/silicon multi-junction solar cell enabled by a silicon tunnel junction," *Appl. Phys. Lett.* **106**(12), 121105 (2015).
- <sup>23</sup>S. Albrecht, M. Saliba, J. P. Correa Baena, F. Lang, L. Kegelmann, M. Mews, L. Steier, A. Abate, J. Rappich, L. Korte, R. Schlatmann, M. K. Nazeeruddin, A. Hagfeldt, M. Grätzel, and B. Rech, "Monolithic perovskite/silicon-heterojunction tandem solar cells processed at low temperature," *Energy Environ. Sci.* **9**(1), 81–88 (2016).
- <sup>24</sup>J. Werner, C. H. Weng, A. Walter, L. Fesquet, J. P. Seif, S. De Wolf, B. Niesen, and C. Ballif, "Efficient monolithic perovskite/silicon tandem solar cell with cell area >1 cm<sup>2</sup>," *J. Phys. Chem. Lett.* **7**(1), 161–166 (2016).
- <sup>25</sup>J. Werner, L. Barraud, A. Walter, M. Bräuninger, F. Sahli, D. Sacchetto, N. Tétreault, B. Paviet-Salomon, S.-J. Moon, C. Allebé, M. Despeisse, S. Nicolay, S. De Wolf, B. Niesen, and C. Ballif, "Efficient near-infrared-transparent perovskite solar cells enabling direct comparison of 4-terminal and monolithic perovskite/silicon tandem cells," *ACS Energy Lett.* **1**, 474–480 (2016).
- <sup>26</sup>J. Werner, A. Walter, E. Rucavado, S.-J. Moon, D. Sacchetto, M. Rienaecker, R. Peibst, R. Brendel, X. Niquille, S. De Wolf, P. Löper, M. Morales-Masis, S. Nicolay, B. Niesen, and C. Ballif, "Zinc tin oxide as high-temperature stable recombination layer for mesoscopic perovskite/silicon monolithic tandem solar cells," *Appl. Phys. Lett.* **109**(23), 233902 (2016).
- <sup>27</sup>F. Sahli, B. A. Kamino, J. Werner, M. Bräuninger, B. Paviet-Salomon, L. Barraud, R. Monnard, J. P. Seif, A. Tomasi, Q. Jeangros, A. Hessler-Wyser, S. De Wolf, M. Despeisse, S. Nicolay, B. Niesen, and C. Ballif, "Improved optics in monolithic perovskite/silicon tandem solar cells with a nanocrystalline silicon recombination junction," *Adv. Energy Mater.* **8**, 1701609 (2017).
- <sup>28</sup>Y. Wu, D. Yan, J. Peng, T. Duong, Y. Wan, P. Phang, H. Shen, N. Wu, C. Barugkin, X. Fu, S. Surve, D. Walter, T. White, K. Catchpole, and K. Weber, "Monolithic perovskite/silicon-homojunction tandem solar cell with over 22% efficiency," *Energy Environ. Sci.* **10**(11), 2472–2479 (2017).
- <sup>29</sup>R. Fan, N. Zhou, L. Zhang, R. Yang, Y. Meng, L. Li, T. Guo, Y. Chen, Z. Xu, G. Zheng, Y. Huang, L. Li, L. Qin, X. Qiu, Q. Chen, and H. Zhou, "Toward full solution processed perovskite/si monolithic tandem solar device with pce exceeding 20%," *Sol. RRL* **1**(11), 1700149 (2017).
- <sup>30</sup>J. Zheng, C. F. J. Lau, H. Mehrvarz, F.-J. Ma, Y. Jiang, X. Deng, A. Sooriyadi, J. Kim, M. Zhang, L. Hu, X. Cui, D. S. Lee, J. Bing, Y. Cho, C. Chen, M. A. Green, S. Huang, and A. W. Y. Ho-Baillie, "Large area efficient interface layer free monolithic perovskite/homo-junction-silicon tandem solar cell with over 20% efficiency," *Energy Environ. Sci.* **11**(9), 2432–2443 (2018).
- <sup>31</sup>F. Sahli, J. Werner, B. A. Kamino, M. Braunerger, R. Monnard, B. Paviet-Salomon, L. Barraud, L. Ding, J. J. Diaz Leon, D. Sacchetto, G. Cattaneo, M. Despeisse, M. Boccard, S. Nicolay, Q. Jeangros, B. Niesen, and C. Ballif, "Fully textured monolithic perovskite/silicon tandem solar cells with 25.2% power conversion efficiency," *Nat. Mater.* **17**(9), 820–826 (2018).
- <sup>32</sup>K. A. Bush, S. Manzoor, K. Frohma, Z. J. Yu, J. A. Raiford, A. F. Palmstrom, H.-P. Wang, R. Prasanna, S. F. Bent, Z. C. Holman, and M. D. McGehee, "Minimizing current and voltage losses to reach 25%-efficient monolithic two-terminal perovskite-silicon tandem solar cells," *ACS Energy Lett.* **3**(9), 2713–2718 (2018).
- <sup>33</sup>J. Zheng, H. Mehrvarz, F.-J. Ma, C.-F. J. Lau, M. Green, S. Huang, and A. W. Y. Ho-Baillie, "21.8% efficient monolithic perovskite/homo-junction-silicon tandem solar cell on 16 cm<sup>2</sup>," *ACS Energy Lett.* **3**(9), 2299–2300 (2018).
- <sup>34</sup>S. Zhu, F. Hou, W. Huang, X. Yao, B. Shi, Q. Ren, J. Chen, L. Yan, S. An, Z. Zhou, H. Ren, C. Wei, Q. Huang, Y. Li, G. Hou, X. Chen, Y. Ding, G. Wang, B. Li, Y. Zhao, and X. Zhang, "Solvent engineering to balance light absorbance and transmittance in perovskite for tandem solar cells," *Sol. RRL* **2**(11), 1800176 (2018).
- <sup>35</sup>Z. Qiu, Z. Xu, N. Li, N. Zhou, Y. Chen, X. Wan, J. Liu, N. Li, X. Hao, P. Bi, Q. Chen, B. Cao, and H. Zhou, "Monolithic perovskite/Si tandem solar cells exceeding 22% efficiency via optimizing top cell absorber," *Nano Energy* **53**, 798–807 (2018).
- <sup>36</sup>B. Chen, Z. Yu, K. Liu, X. Zheng, Y. Liu, J. Shi, D. Spronk, P. N. Rudd, Z. Holman, and J. Huang, "Grain engineering for perovskite/silicon monolithic tandem solar cells with efficiency of 25.4%," *Joule* **3**(1), 177–190 (2018).
- <sup>37</sup>M. Jošt, E. Köhnen, A. Morales Vilches, B. Lipovšek, K. Jäger, B. Macco, A. Al-Ashouri, J. Krc, L. Korte, B. Rech, R. Schlatmann, M. Topic, B. Stannowski, and S. Albrecht, "Textured interfaces in monolithic perovskite/silicon tandem solar cells: Advanced light management for improved efficiency and energy yield," *Energy Environ. Sci.* **11**(12), 3511–3523 (2019).
- <sup>38</sup>See <https://www.oxfordpv.com/news/oxford-pv-sets-world-record-perovskite-solar-cell> for Oxford PV.
- <sup>39</sup>M. A. Green, E. D. Dunlop, D. H. Levi, J. Hohl-Ebinger, M. Yoshita, and A. W. Y. Ho-Baillie, "Solar cell efficiency tables (version 54)," *IEEE J. Photovoltaics* **27**(7), 565–575 (2019).
- <sup>40</sup>F. Hou, C. Han, O. Isabella, L. Yan, B. Shi, J. Chen, S. An, Z. Zhou, W. Huang, H. Ren, Q. Huang, G. Hou, X. Chen, Y. Li, Y. Ding, G. Wang, C. Wei, D. Zhang, M. Zeman, Y. Zhao, and X. Zhang, "Inverted pyramidal-textured PDMS antireflective foils for perovskite/silicon tandem solar cells with flat top cell," *Nano Energy* **56**, 234–240 (2019).
- <sup>41</sup>H. Shen, S. T. Omelchenko, D. A. Jacobs, S. Yalamanchili, Y. Wan, D. Yan, P. Phang, T. Duong, Y. Wu, Y. Yin, C. Samundsett, J. Peng, N. Wu, T. P. White, G. G. Andersson, N. S. Lewis, and K. R. Catchpole, "In situ recombination junction between p-Si and TiO<sub>2</sub> enables high-efficiency monolithic perovskite/Si tandem cells," *Sci. Adv.* **4**(12), eaau9711 (2018).
- <sup>42</sup>F. Hou, L. Yan, B. Shi, J. Chen, S. Zhu, Q. Ren, S. An, Z. Zhou, H. Ren, C. Wei, Q. Huang, G. Hou, X. Chen, Y. Li, Y. Ding, G. Wang, D. Zhang, Y. Zhao, and X. Zhang, "Monolithic perovskite/silicon-heterojunction tandem solar cells with open-circuit voltage of over 1.8 V," *ACS Appl. Energy Mater.* **2**(1), 243–249 (2019).
- <sup>43</sup>L. Mazzarella, Y.-H. Lin, S. Kirner, A. B. Morales-Vilches, L. Korte, S. Albrecht, E. Crossland, B. Stannowski, C. Case, H. J. Snaith, and R. Schlatmann, "Infrared light management using a nanocrystalline silicon oxide interlayer in monolithic perovskite/silicon heterojunction tandem solar cells with efficiency above 25%," *Adv. Energy Mater.* **9**, 1803241 (2019).

- <sup>44</sup>G. Nogay, F. Sahli, J. Werner, R. Monnard, M. Boccard, M. Despeisse, F.-J. Haug, Q. Jeangros, A. Ingenito, and C. Ballif, “25.1%-efficient monolithic perovskite/silicon tandem solar cell based on a p-type mono-crystalline textured silicon wafer and high temperature passivating contacts,” *ACS Energy Lett.* **4**(4), 844–845 (2019).
- <sup>45</sup>C. U. Kim, J. C. Yu, E. D. Jung, I. Y. Choi, W. Park, H. Lee, I. Kim, D.-K. Lee, K. K. Hong, and M. H. Song, “Optimization of device design for low cost and high efficiency planar monolithic perovskite/silicon tandem solar cells,” *Nano Energy* **60**, 213–221 (2019).
- <sup>46</sup>B. Kamino, B. Paviet-Salomon, S.-J. Moon, N. Badel, J. Levrat, G. Christmann, A. Walter, A. Faes, L. Ding, J. J. Diaz Leon, A. Paracchino, M. Despeisse, C. Ballif, and S. Nicolay, “Low temperature screen-print metallization for the scale up of 2-terminal perovskite-silicon tandems,” *ACS Appl. Energy Mater.* **2**(5), 3815–3821 (2019).
- <sup>47</sup>E. Köhnen, M. Jošt, A. B. Morales-Vilches, P. Tockhorn, A. Al-Ashouri, B. Macco, L. Kegelmann, L. Korte, B. Rech, R. Schlatmann, B. Stannowski, and S. Albrecht, “Highly efficient monolithic perovskite silicon tandem solar cells: Analyzing the influence of current mismatch on device performance,” *Sustainable Energy Fuels* **3**(8), 1995–2005 (2019).
- <sup>48</sup>C. O. Ramírez Quiroz, G. D. Spyropoulos, M. Salvador, L. M. Roch, M. Berlinghof, J. Darío Perea, K. Forberich, L. I. Dion-Bertrand, N. J. Schrenker, A. Classen, N. Gasparini, G. Chistiakova, M. Mews, L. Korte, B. Rech, N. Li, F. Hauke, E. Spiecker, T. Ameri, S. Albrecht, G. Abellán, S. León, T. Unruh, A. Hirsch, A. Aspuru-Guzik, and C. J. Brabec, “Interface molecular engineering for laminated monolithic perovskite/silicon tandem solar cells with 80.4% fill factor,” *Adv. Funct. Mater.* **29**(40), 1901476 (2019).
- <sup>49</sup>A. J. Bett, P. S. C. Schulze, K. M. Winkler, Ö. S. Kabaklı, I. Ketterer, L. E. Mundt, S. K. Reichmuth, G. Siefer, L. Cojocaru, L. Tutsch, M. Bivour, M. Hermle, S. W. Glunz, and J. C. Goldschmidt, “Two-terminal perovskite silicon tandem solar cells with a high-bandgap perovskite absorber enabling voltages over 1.8 V,” *Prog. Photovoltaics* **28**(2), 99–110 (2019).
- <sup>50</sup>B. Chen, Z. J. Yu, S. Manzoor, S. Wang, W. Weigand, Z. Yu, G. Yang, Z. Ni, X. Dai, Z. C. Holman, and J. Huang, “Blade-coated perovskites on textured silicon for 26%-efficient monolithic perovskite/silicon tandem solar cells,” *Joule* **4**(4), 850–864 (2020).
- <sup>51</sup>Y. Hou, E. Aydin, M. De Bastiani, C. Xiao, F. H. Isikgor, D.-J. Xue, B. Chen, H. Chen, B. Bahrami, and A. H. Chowdhury, “Efficient tandem solar cells with solution-processed perovskite on textured crystalline silicon,” *Science* **367**(6482), 1135–1140 (2020).
- <sup>52</sup>J. Xu, C. C. Boyd, J. Y. Zhengshan, A. F. Palmstrom, D. J. Witter, B. W. Larson, R. M. France, J. Werner, S. P. Harvey, and E. J. Wolf, “Triple-halide wide-band gap perovskites with suppressed phase segregation for efficient tandems,” *Science* **367**(6482), 1097–1104 (2020).
- <sup>53</sup>D. Kim, H. J. Jung, I. J. Park, B. W. Larson, S. P. Dunfield, C. Xiao, J. Kim, J. Tong, P. Boonmongkolras, S. G. Ji, F. Zhang, S. R. Pae, M. Kim, S. B. Kang, V. Dravid, J. J. Berry, J. Y. Kim, K. Zhu, D. H. Kim, and B. Shin, “Efficient, stable silicon tandem cells enabled by anion-engineered wide-bandgap perovskites,” *Science* **368**(6487), 155–160 (2020).
- <sup>54</sup>P. S. C. Schulze, A. J. Bett, M. Bivour, P. Caprioglio, F. M. Gerspacher, Ö. S. Kabaklı, A. Richter, M. Stolterfoht, Q. Zhang, D. Neher, M. Hermle, H. Hillebrecht, S. W. Glunz, and J. C. Goldschmidt, “25.1% high-efficient monolithic perovskite silicon tandem solar cell with a high band gap perovskite absorber,” *Sol. RRL* **4**(7), 2000152 (2020).
- <sup>55</sup>A. S. Subbiah, F. H. Isikgor, C. T. Howells, M. De Bastiani, J. Liu, E. Aydin, F. Furlan, T. G. Allen, F. Xu, S. Zhumagali, S. Hoogland, E. H. Sargent, I. McCulloch, and S. D. Wolf, “High-performance perovskite single-junction and textured perovskite/silicon tandem solar cells via slot-die-coating,” *ACS Energy Lett.* **5**(9), 3034–3040 (2020).
- <sup>56</sup>E. Aydin, T. G. Allen, M. De Bastiani, L. Xu, J. Ávila, M. Salvador, E. Van Kerschaver, and S. D. Wolf, “Interplay between temperature and bandgap energies on the outdoor performance of perovskite/silicon tandem solar cells,” *Nat. Energy* **5**(11), 851–859 (2020).
- <sup>57</sup>M. D. Bastiani, A. J. Mirabelli, Y. Hou, F. Gota, E. Aydin, T. G. Allen, J. Troughton, A. S. Subbiah, F. H. Isikgor, J. Liu, L. Xu, B. Chen, E. Van Kerschaver, D. Baran, B. Fraboni, M. F. Salvador, U. W. Paetzold, E. H. Sargent, and S. D. Wolf, “Efficient bifacial monolithic perovskite/silicon tandem solar cells via bandgap engineering,” *Nat. Energy* **6**, 167–175 (2021).
- <sup>58</sup>T. Todorov, T. Gershon, O. Gunawan, Y. S. Lee, C. Sturdevant, L. Y. Chang, and S. Guha, “Monolithic perovskite-cigs tandem solar cells via *in situ* band gap engineering,” *Adv. Energy Mater.* **5**(23), 1500799 (2015).
- <sup>59</sup>M. Jost, T. Bertram, D. Koushik, J. Marquez, M. Verheijen, M. D. Heinemann, E. Köhnen, A. Al-Ashouri, S. Braunger, F. Lang, B. Rech, T. Unold, M. Creatore, I. Lauerma, C. A. Kaufmann, R. Schlatmann, and S. Albrecht, “21.6%-efficient monolithic perovskite/Cu(In,Ga)Se<sub>2</sub> tandem solar cells with thin conformal hole transport layers for integration on rough bottom cell surfaces,” *ACS Energy Lett.* **4**(2), 583–590 (2019).
- <sup>60</sup>A. Al-Ashouri, A. Magomedov, M. Roß, M. Jošt, M. Talaikis, G. Chistiakova, T. Bertram, J. A. Márquez, E. Köhnen, E. Kasparavičius, S. Levenco, L. Gil-Escrí, C. J. Hages, R. Schlatmann, B. Rech, T. Malinauskas, T. Unold, C. A. Kaufmann, L. Korte, G. Niaura, V. Getautis, and S. Albrecht, “Conformal monolayer contacts with lossless interfaces for perovskite single junction and monolithic tandem solar cells,” *Energy Environ. Sci.* **12**(11), 3356–3369 (2019).
- <sup>61</sup>F. Fu, S. Nishiwaki, J. Werner, T. Feurer, S. Pisoni, Q. Jeangros, S. Buecheler, C. Ballif, and A. N. Tiwari, “Flexible perovskite/Cu (In, Ga) Se<sub>2</sub> monolithic tandem solar cells,” *arXiv:1907.10330* (2019).
- <sup>62</sup>T. J. Jacobsson, A. Hultqvist, S. Svanström, L. Riekehr, U. B. Cappel, E. Unger, H. Rensmo, E. M. J. Johansson, M. Edoff, and G. Boschloo, “2-Terminal CIGS-perovskite tandem cells: A layer by layer exploration,” *Sol. Energy* **207**, 270–288 (2020).
- <sup>63</sup>M. Jošt, A. Al-Ashouri, B. Lipovšek, T. Bertram, R. Schlatmann, C. A. Kaufmann, M. Topič, and S. Albrecht, “Perovskite/CIGS tandem solar cells—Can they catch up with perovskite/c-Si tandems?,” in 47th IEEE Photovoltaic Specialists Conference (PVSC) (2020).
- <sup>64</sup>F. Jiang, T. Liu, B. Luo, J. Tong, F. Qin, S. Xiong, Z. Li, and Y. Zhou, “A two-terminal perovskite/perovskite tandem solar cell,” *J. Mater. Chem. A* **4**(4), 1208–1213 (2016).
- <sup>65</sup>J. H. Heo and S. H. Im, “CH<sub>3</sub>NH<sub>3</sub>PbBr<sub>3</sub>–CH<sub>3</sub>NH<sub>3</sub>PbI<sub>3</sub> perovskite–perovskite tandem solar cells with exceeding 2.2 V open circuit voltage,” *Adv. Mater.* **28**(25), 5121–5125 (2016).
- <sup>66</sup>G. E. Eperon, T. Leijtens, K. A. Bush, R. Prasanna, T. Green, J. T.-W. Wang, D. P. McMeekin, G. Volonakis, R. L. Milot, and R. May, “Perovskite–perovskite tandem photovoltaics with optimized band gaps,” *Science* **354**(6314), 861–865 (2016).
- <sup>67</sup>D. Forgács, L. Gil-Escrí, D. Pérez-Del-Rey, C. Momblona, J. Werner, B. Niesen, C. Ballif, M. Sessolo, and H. J. Bolink, “Efficient monolithic perovskite/perovskite tandem solar cells,” *Adv. Energy Mater.* **7**(8), 1602121 (2017).
- <sup>68</sup>A. Rajagopal, Z. Yang, S. B. Jo, I. L. Braly, P. W. Liang, H. W. Hillhouse, and A. K. Jen, “Highly efficient perovskite–perovskite tandem solar cells reaching 80% of the theoretical limit in photovoltage,” *Adv. Mater.* **29**(34), 1702140 (2017).
- <sup>69</sup>T. Leijtens, R. Prasanna, K. A. Bush, G. E. Eperon, J. A. Raiford, A. Gold-Parker, E. J. Wolf, S. A. Swifter, C. C. Boyd, H.-P. Wang, M. F. Toney, S. F. Bent, and M. D. McGeehee, “Tin-lead halide perovskites with improved thermal and air stability for efficient all-perovskite tandem solar cells,” *Sustainable Energy Fuels* **2**(11), 2450–2459 (2018).
- <sup>70</sup>J. Ávila, C. Momblona, P. Boix, M. Sessolo, M. Anaya, G. Lozano, K. Vandewal, H. Miguez, and H. J. Bolink, “High voltage vacuum-deposited CH<sub>3</sub>NH<sub>3</sub>PbI<sub>3</sub>–CH<sub>3</sub>NH<sub>3</sub>PbI<sub>3</sub> tandem solar cells,” *Energy Environ. Sci.* **11**(11), 3292–3297 (2018).
- <sup>71</sup>C. Li, Z. S. Wang, H. L. Zhu, D. Zhang, J. Cheng, H. Lin, D. Ouyang, and W. C. H. Choy, “Thermionic emission-based interconnecting layer featuring solvent resistance for monolithic tandem solar cells with solution-processed perovskites,” *Adv. Energy Mater.* **8**(36), 1801954 (2018).
- <sup>72</sup>C.-Y. Chang, B.-C. Tsai, Y.-C. Hsiao, M.-Z. Lin, and H.-F. Meng, “Solution-processed conductive interconnecting layer for highly-efficient and long-term stable monolithic perovskite tandem solar cells,” *Nano Energy* **55**, 354–367 (2019).
- <sup>73</sup>D. Zhao, C. Chen, C. Wang, M. M. Junda, Z. Song, C. R. Grice, Y. Yu, C. Li, B. Subedi, N. J. Podraza, X. Zhao, G. Fang, R.-G. Xiong, K. Zhu, and Y. Yan, “Efficient two-terminal all-perovskite tandem solar cells enabled by high-quality low-bandgap absorber layers,” *Nat. Energy* **3**, 1093 (2018).

- <sup>74</sup>J. Tong, Z. Song, D. H. Kim, X. Chen, C. Chen, A. F. Palmstrom, P. F. Ndione, M. O. Reese, S. P. Dunfield, and O. G. Reid, "Carrier lifetimes of >1  $\mu$ s in Sn-Pb perovskites enable efficient all-perovskite tandem solar cells," *Science* **364**(6439), 475–479 (2019).
- <sup>75</sup>A. F. Palmstrom, G. E. Eperon, T. Leijtens, R. Prasanna, S. N. Habisreutinger, W. Nemeth, E. A. Gaillard, S. P. Dunfield, M. Reese, S. Nanayakkara, T. Moot, J. Werner, J. Liu, B. To, S. T. Christensen, M. D. McGehee, M. F. A. M. van Hest, J. M. Luther, J. J. Berry, and D. T. Moore, "Enabling flexible all-perovskite tandem solar cells," *Joule* **3**(9), 2193–2204 (2019).
- <sup>76</sup>Z. Yang, Z. Yu, H. Wei, X. Xiao, Z. Ni, B. Chen, Y. Deng, S. N. Habisreutinger, X. Chen, K. Wang, J. Zhao, P. N. Rudd, J. J. Berry, M. C. Beard, and J. Huang, "Enhancing electron diffusion length in narrow-bandgap perovskites for efficient monolithic perovskite tandem solar cells," *Nat. Commun.* **10**(1), 4498 (2019).
- <sup>77</sup>M. Wei, K. Xiao, G. Walters, R. Lin, Y. Zhao, M. I. Saidaminov, P. Todorovic, A. Johnston, Z. Huang, H. Chen, A. Li, J. Zhu, Z. Yang, Y. K. Wang, A. H. Proppe, S. O. Kelley, Y. Hou, O. Voznyy, H. Tan, and E. H. Sargent, "Combining efficiency and stability in mixed tin-lead perovskite solar cells by capping grains with an ultrathin 2D layer," *Adv. Mater.* **32**(12), 1907058 (2020).
- <sup>78</sup>Z. Song, D. Zhao, C. Chen, R. H. Ahangharnejad, C. Li, K. Ghimire, N. J. Podraza, M. J. Heben, K. Zhu, and Y. Yan, paper presented at the 2019 IEEE 46th Photovoltaic Specialists Conference (PVSC) (2019).
- <sup>79</sup>Z. Yu, Z. Yang, Z. Ni, Y. Shao, B. Chen, Y. Lin, H. Wei, J. Y. Zhengshan, Z. Holman, and J. Huang, "Simplified interconnection structure based on  $C_{60}/SnO_{2-x}$  for all-perovskite tandem solar cells," *Nat. Energy* **5**(9), 657–665 (2020).
- <sup>80</sup>K. Xiao, R. Lin, Q. Han, Y. Hou, Z. Qin, H. T. Nguyen, J. Wen, M. Wei, V. Yeddu, M. I. Saidaminov, Y. Gao, X. Luo, Y. Wang, H. Gao, C. Zhang, J. Xu, J. Zhu, E. H. Sargent, and H. Tan, "All-perovskite tandem solar cells with 24.2% certified efficiency and area over 1 cm<sup>2</sup> using surface-anchoring zwitterionic antioxidant," *Nat. Energy* **5**(11), 870–880 (2020).
- <sup>81</sup>C. Li, Z. Song, C. Chen, C. Xiao, B. Subedi, S. P. Harvey, N. Shrestha, K. K. Subedi, L. Chen, D. Liu, Y. Li, Y.-W. Kim, C.-s Jiang, M. J. Heben, D. Zhao, R. J. Ellingson, N. J. Podraza, M. Al-Jassim, and Y. Yan, "Low-bandgap mixed tin-lead iodide perovskites with reduced methylammonium for simultaneous enhancement of solar cell efficiency and stability," *Nat. Energy* **5**(10), 768–776 (2020).
- <sup>82</sup>C.-C. Chen, S.-H. Bae, W.-H. Chang, Z. Hong, G. Li, Q. Chen, H. Zhou, and Y. Yang, "Perovskite/polymer monolithic hybrid tandem solar cells utilizing a low-temperature, full solution process," *Mater. Horiz.* **2**(2), 203–211 (2015).
- <sup>83</sup>Y. Liu, L. A. Renna, M. Bag, Z. A. Page, P. Kim, J. Choi, T. Emrick, D. Venkataraman, and T. P. Russell, "High efficiency tandem thin-perovskite/polymer solar cells with a graded recombination layer," *ACS Appl. Mater. Interfaces* **8**(11), 7070–7076 (2016).
- <sup>84</sup>Z. Li, S. Wu, J. Zhang, K. C. Lee, H. Lei, F. Lin, Z. Wang, Z. Zhu, and A. K. Y. Jen, "Hybrid perovskite-organic flexible tandem solar cell enabling highly efficient electrocatalysis overall water splitting," *Adv. Energy Mater.* **10**(18), 2000361 (2020).
- <sup>85</sup>K. A. Bush, A. F. Palmstrom, Z. J. Yu, M. Boccard, R. Cheacharoen, J. P. Mailoa, D. P. McMeekin, R. L. Z. Hoye, C. D. Bailie, T. Leijtens, I. M. Peters, M. C. Minichetti, N. Rolston, R. Prasanna, S. Sofia, D. Harwood, W. Ma, F. Moghadam, H. J. Snaith, T. Buonassisi, Z. C. Holman, S. F. Bent, and M. D. McGehee, "23.6%-efficient monolithic perovskite/silicon tandem solar cells with improved stability," *Nat. Energy* **2**(4), 17009 (2017).
- <sup>86</sup>E. Köhnen, P. Wagner, F. Lang, A. Cruz, B. Li, M. Roß, M. Jošt, A. B. Morales-Vilches, M. Topič, M. Stolterfoht, D. Neher, L. Korte, B. Rech, R. Schlatmann, B. Stannowski, and S. Albrecht, "27.9% efficient monolithic perovskite/silicon tandem solar cells on industry compatible bottom cells," *Sol. RRL* **5**, 2100244 (2021).
- <sup>87</sup>F. H. Isikgor, F. Furlan, J. Liu, E. Ugur, M. K. Eswaran, A. S. Subbiah, E. Yengel, M. D. Bastiani, G. T. Harrison, and S. J. J. Zhumagali, "Concurrent cationic and anionic perovskite defect passivation enables 27.4% perovskite/silicon tandems with suppression of halide segregation," *Joule* **5**(6), 1566–1586 (2021).
- <sup>88</sup>C. Case, "The path to perovskite performance and production (conference presentation)," *Proc. SPIE* **10737**, 1073701 (2018).
- <sup>89</sup>M. Green, E. Dunlop, J. Hohl-Ebinger, M. Yoshita, N. Kopidakis, and X. Hao, "Solar cell efficiency tables (version 57)," *Prog. Photovoltaics* **29**(1), 3–15 (2020).
- <sup>90</sup>N. L. Chang, J. Zheng, Y. Wu, H. Shen, F. Qi, K. Catchpole, A. Ho-Baillie, and R. J. Egan, "A bottom-up cost analysis of silicon-perovskite tandem photovoltaics," *Prog. Photovoltaics* **29**(3), 401–413 (2021).
- <sup>91</sup>A. Richter, R. Müller, J. Benick, P. Feldmann, B. Steinhäuser, C. Reichel, A. Fell, M. Bivour, M. Hermle, and S. W. Glunz, "Design rules for high-efficiency both-sides-contacted silicon solar cells with balanced charge carrier transport and recombination losses," *Nat. Energy* **6**(4), 429–438 (2021).
- <sup>92</sup>J. Zheng, H. Mehrvarz, C. Liao, J. Bing, X. Cui, Y. Li, V. R. Gonçales, C.-F. J. Lau, D. S. Lee, Y. Li, M. Zhang, J. Kim, Y. Cho, L. G. Caro, S. Tang, C. Chen, S. Huang, and A. W. Y. Ho-Baillie, "Large area 23%-efficient monolithic perovskite/homo-junction-silicon tandem solar cell with enhanced UV stability using down-shifting material," *ACS Energy Lett.* **4**(11), 2623–2631 (2019).
- <sup>93</sup>A. Ho-Baillie, "Perovskites cover silicon textures," *Nat. Mater.* **17**(9), 751–752 (2018).
- <sup>94</sup>M. T. Hörtanner and H. J. Snaith, "Predicting and optimising the energy yield of perovskite-on-silicon tandem solar cells under real world conditions," *Energy Environ. Sci.* **10**(9), 1983–1993 (2017).
- <sup>95</sup>Y. P. Varshni, "Temperature dependence of the energy gap in semiconductors," *Physica* **34**(1), 149–154 (1967).
- <sup>96</sup>M. A. Green, Y. Jiang, A. M. Soufiani, and A. Ho-Baillie, "Optical properties of photovoltaic organic-inorganic lead halide perovskites," *J. Phys. Chem. Lett.* **6**(23), 4774–4785 (2015).
- <sup>97</sup>R. A. Jishi, O. B. Ta, and A. A. Sharif, "Modeling of lead halide perovskites for photovoltaic applications," *J. Phys. Chem. C* **118**(49), 28344–28349 (2014).
- <sup>98</sup>J. Kim, J. S. Yun, Y. Cho, D. S. Lee, B. Wilkinson, A. M. Soufiani, X. Deng, J. Zheng, A. Shi, S. Lim, S. Chen, Z. Hameiri, M. Zhang, C. F. J. Lau, S. Huang, M. A. Green, and A. W. Y. Ho-Baillie, "Overcoming the challenges of large-area high-efficiency perovskite solar cells," *ACS Energy Lett.* **2**(9), 1978–1984 (2017).
- <sup>99</sup>D. Li, D. Zhang, K. S. Lim, Y. Hu, Y. Rong, A. Mei, N. G. Park, and H. Han, "A review on scaling up perovskite solar cells," *Adv. Funct. Mater.* **31**(12), 2008621 (2020).
- <sup>100</sup>M. A. Green, E. D. Dunlop, J. Hohl-Ebinger, M. Yoshita, N. Kopidakis, and X. Hao, "Solar cell efficiency tables (version 58)," *Prog. Photovoltaics* **29**, 657 (2021).
- <sup>101</sup>T. D. Lee and A. U. Ebong, "A review of thin film solar cell technologies and challenges," *Renewable Sustainable Energy Rev.* **70**, 1286–1297 (2017).
- <sup>102</sup>T. Todorov, T. Gershon, O. Gunawan, C. Sturdevant, and S. Guha, "Perovskite-kesterite monolithic tandem solar cells with high open-circuit voltage," *Appl. Phys. Lett.* **105**(17), 173902 (2014).
- <sup>103</sup>M. Jošt, A. Al-Ashouri, B. Lipovsek, T. Bertram, R. Schlatmann, C. A. Kaufmann, M. Topič, and S. Albrecht, paper presented at the 2020 47th IEEE Photovoltaic Specialists Conference (PVSC) (2020).
- <sup>104</sup>X. Xu, J. Xiao, G. Zhang, L. Wei, X. Jiao, H.-L. Yip, and Y. Cao, "Interface-enhanced organic solar cells with extrapolated T80 lifetimes of over 20 years," *Sci. Bull.* **65**(3), 208–216 (2020).
- <sup>105</sup>W. Yang, Z. Luo, R. Sun, J. Guo, T. Wang, Y. Wu, W. Wang, J. Guo, Q. Wu, and M. Shi, "Simultaneous enhanced efficiency and thermal stability in organic solar cells from a polymer acceptor additive," *Nat. Commun.* **11**(1), 1218 (2020).
- <sup>106</sup>C. C. Stoumpos, C. D. Malliakas, and M. G. Kanatzidis, "Semiconducting tin and lead iodide perovskites with organic cations: Phase transitions, high mobilities, and near-infrared photoluminescent properties," *Inorg. Chem.* **52**(15), 9019–9038 (2013).
- <sup>107</sup>L. Ma, F. Hao, C. C. Stoumpos, B. T. Phelan, M. R. Wasielewski, and M. G. Kanatzidis, "Carrier diffusion lengths of over 500 nm in lead-free perovskite  $CH_3NH_3SnI_3$  films," *J. Am. Chem. Soc.* **138**(44), 14750–14755 (2016).
- <sup>108</sup>A. M. Igual-Muñoz, J. Ávila, P. P. Boix, and H. J. Bolink, "FAPb<sub>0.5</sub>Sn<sub>0.5</sub>I<sub>3</sub>: A narrow bandgap perovskite synthesized through evaporation methods for solar cell applications," *Solar RRL* **4**(2), 1900283 (2020).
- <sup>109</sup>J. M. Ball, L. Buizza, H. C. Sansom, M. D. Farrar, M. T. Klug, J. Borchert, J. Patel, L. M. Herz, M. B. Johnston, and H. J. A. E. L. Snaith, "Dual-source coevaporation of low-bandgap FA<sub>1-x</sub>Cs<sub>x</sub>Sn<sub>1-y</sub>Pb<sub>y</sub>I<sub>3</sub> perovskites for photovoltaics," *ACS Energy Lett.* **4**(11), 2748–2756 (2019).

- <sup>110</sup>H. Choubisa, M. Askerka, K. Ryczko, O. Voznyy, K. Mills, I. Tamblyn, and E. H. J. M. Sargent, "Crystal site feature embedding enables exploration of large chemical spaces," *Matter* **3**(2), 433–448 (2020).
- <sup>111</sup>R. Sheng, M. T. Hoerantner, Z. Wang, Y. Jiang, W. Zhang, A. Agosti, S. Huang, X. Hao, A. W. Y. Ho-Baillie, M. A. Green, and H. J. Snaith, "Monolithic wide band gap perovskite/perovskite tandem solar cells with organic recombination layers," *J. Phys. Chem. C* **121**(49), 27256–27262 (2017).
- <sup>112</sup>D. P. McMeekin, S. Mahesh, N. K. Noel, M. T. Klug, J. Lim, J. H. Warby, J. M. Ball, L. M. Herz, M. B. Johnston, and H. J. Snaith, "Solution-processed all-perovskite multi-junction solar cells," *Joule* **3**(2), 387–401 (2019).
- <sup>113</sup>K. Xiao, J. Wen, Q. Han, R. Lin, Y. Gao, S. Gu, Y. Zang, Y. Nie, J. Zhu, J. Xu, and H. Tan, "Solution-processed monolithic all-perovskite triple-junction solar cells with efficiency exceeding 20%," *ACS Energy Lett.* **5**(9), 2819–2826 (2020).
- <sup>114</sup>J. Wang, V. Zardetto, K. Datta, D. Zhang, M. M. Wienk, and R. A. Janssen, "16.8% Monolithic all-perovskite triple-junction solar cells via a universal two-step solution process," *Nat. Commun.* **11**(1), 5254 (2020).
- <sup>115</sup>J. Werner, F. Sahli, F. Fu, J. J. Diaz Leon, A. Walter, B. A. Kamino, B. Niesen, S. Nicolay, Q. Jeangros, and C. Ballif, "Perovskite/perovskite/silicon monolithic triple-junction solar cells with a fully textured design," *ACS Energy Lett.* **3**(9), 2052–2058 (2018).
- <sup>116</sup>A. S. Brown and M. A. Green, "Detailed balance limit for the series constrained two terminal tandem solar cell," *Phys. E* **14**(1–2), 96–100 (2002).
- <sup>117</sup>A. D. Vos, "Detailed balance limit of the efficiency of tandem solar cells," *J. Phys. D* **13**(5), 839 (1980).
- <sup>118</sup>M. T. Hörtner, T. Leijtens, M. E. Ziffer, G. E. Eperon, M. G. Christoforo, M. D. McGehee, and H. J. Snaith, "The potential of multijunction perovskite solar cells," *ACS Energy Lett.* **2**(10), 2506–2513 (2017).
- <sup>119</sup>H. Li and W. Zhang, "Perovskite tandem solar cells: From fundamentals to commercial deployment," *Chem. Rev.* **120**(18), 9835–9950 (2020).
- <sup>120</sup>D. J. Slotcavage, H. I. Karunadasa, and M. D. McGehee, "Light-induced phase segregation in halide-perovskite absorbers," *ACS Energy Lett.* **1**(6), 1199–1205 (2016).
- <sup>121</sup>W. Mao, C. R. Hall, S. Bernardi, Y.-B. Cheng, A. Widmer-Cooper, T. A. Smith, and U. J. N. m Bach, "Light-induced reversal of ion segregation in mixed-halide perovskites," *Nat. Mater.* **20**(1), 55–61 (2021).
- <sup>122</sup>A. Ho-Baillie, M. Zhang, C. F. J. Lau, F.-J. Ma, and S. Huang, "Untapped potentials of inorganic metal halide perovskite solar cells," *Joule* **3**(4), 938–955 (2019).
- <sup>123</sup>J. Zhang, Z. Wang, A. Mishra, M. Yu, M. Shasti, W. Tress, D. J. Kubicki, C. E. Avalos, H. Lu, and Y. Liu, "Intermediate phase enhances inorganic perovskite and metal oxide interface for efficient photovoltaics," *Joule* **4**(1), 222–234 (2020).
- <sup>124</sup>Y. Zhou, Y. H. Jia, H. H. Fang, M. A. Loi, F. Y. Xie, L. Gong, M. C. Qin, X. H. Lu, C. P. Wong, and N. Zhao, "Composition-tuned wide bandgap perovskites: From grain engineering to stability and performance improvement," *Adv. Funct. Mater.* **28**(35), 1803130 (2018).
- <sup>125</sup>S. Gharibzadeh, B. Abdollahi Nejand, M. Jakoby, T. Abzieher, D. Hauschild, S. Moghadamzadeh, J. A. Schwenzer, P. Brenner, R. Schmager, and A. A. Haghhighirad, "Record open-circuit voltage wide-bandgap perovskite solar cells utilizing 2D/3D perovskite heterostructure," *Adv. Energy Mater.* **9**(21), 1803699 (2019).
- <sup>126</sup>W.-Q. Wu, Z. Yang, P. N. Rudd, Y. Shao, X. Dai, H. Wei, J. Zhao, Y. Fang, Q. Wang, and Y. Liu, "Bilateral alkylamine for suppressing charge recombination and improving stability in blade-coated perovskite solar cells," *Sci. Adv.* **5**(3), eaav8925 (2019).
- <sup>127</sup>M. A. Mahmud, T. Duong, Y. Yin, J. Peng, Y. Wu, T. Lu, H. T. Pham, H. Shen, D. Walter, and H. T. Nguyen, "In situ formation of mixed-dimensional surface passivation layers in perovskite solar cells with dual-isomer alkylammonium cations," *Small* **16**(49), 2005022 (2020).
- <sup>128</sup>W. Xiang, Z. Wang, D. J. Kubicki, X. Wang, W. Tress, J. Luo, J. Zhang, A. Hofstetter, L. Zhang, and L. Emsley, "Ba-induced phase segregation and band gap reduction in mixed-halide inorganic perovskite solar cells," *Nat. Commun.* **10**(1), 4686 (2019).
- <sup>129</sup>W. Xiang, Z. Wang, D. J. Kubicki, W. Tress, J. Luo, D. Prochowicz, S. Akin, L. Emsley, J. Zhou, G. Dietler, M. Grätzel, and A. Hagfeldt, "Europium-doped CsPbI<sub>2</sub>Br for stable and highly efficient inorganic perovskite solar cells," *Joule* **3**(1), 205–214 (2018).
- <sup>130</sup>L. Wang, H. Zhou, J. Hu, B. Huang, M. Sun, B. Dong, G. Zheng, Y. Huang, Y. Chen, L. Li, Z. Xu, N. Li, Z. Liu, Q. Chen, L.-D. Sun, and C.-H. Yan, "A Eu<sup>3+</sup>-Eu<sup>2+</sup> ion redox shuttle imparts operational durability to Pb-I perovskite solar cells," *Science* **363**(6424), 265–270 (2019).
- <sup>131</sup>F. Zheng, W. Chen, T. Bu, K. P. Ghiggino, F. Huang, Y. Cheng, P. Tapping, T. W. Kee, B. Jia, and X. Wen, "Triggering the passivation effect of potassium doping in mixed-cation mixed-halide perovskite by light illumination," *Adv. Energy Mater.* **9**(24), 1901016 (2019).
- <sup>132</sup>M. A. Mahmud, T. Duong, Y. Yin, H. T. Pham, D. Walter, J. Peng, Y. Wu, L. Li, H. Shen, and N. Wu, "Double-sided surface passivation of 3D perovskite film for high-efficiency mixed-dimensional perovskite solar cells," *Adv. Funct. Mater.* **30**(7), 1907962 (2020).
- <sup>133</sup>K. Choi, J. Lee, H. I. Kim, C. W. Park, G.-W. Kim, H. Choi, S. Park, S. A. Park, and T. Park, "Thermally stable, planar hybrid perovskite solar cells with high efficiency," *Energy Environ. Sci.* **11**(11), 3238–3247 (2018).
- <sup>134</sup>H. Wang, S. Cao, B. Yang, H. Li, M. Wang, X. Hu, K. Sun, and Z. Zang, "NH<sub>4</sub>Cl-Modified ZnO for high-performance CsPbIBr<sub>2</sub> perovskite solar cells via low-temperature process," *Sol. RRL* **4**(1), 1900363 (2020).
- <sup>135</sup>P. Cui, D. Wei, J. Ji, H. Huang, E. Jia, S. Dou, T. Wang, W. Wang, and M. Li, "Planar p-n homojunction perovskite solar cells with efficiency exceeding 21.3%," *Nat. Energy* **4**(2), 150–159 (2019).
- <sup>136</sup>X. Zhao, C. Yao, T. Liu, J. C. Hamill, Jr., G. O. Ngongang Ndjawo, G. Cheng, N. Yao, H. Meng, and Y. L. Loo, "Extending the photovoltaic response of perovskite solar cells into the near-infrared with a narrow-bandgap organic semiconductor," *Adv. Mater.* **31**(49), 1904494 (2019).
- <sup>137</sup>N. J. Jeon, J. H. Noh, Y. C. Kim, W. S. Yang, S. Ryu, and S. I. Seok, "Solvent engineering for high-performance inorganic–organic hybrid perovskite solar cells," *Nat. Mater.* **13**(9), 897–903 (2014).
- <sup>138</sup>J. H. Noh, S. H. Im, J. H. Heo, T. N. Mandal, and S. I. Seok, "Chemical management for colorful, efficient, and stable inorganic–organic hybrid nanostructured solar cells," *Nano Lett.* **13**(4), 1764–1769 (2013).
- <sup>139</sup>S. A. Kulkarni, T. Baikie, P. P. Boix, N. Yantara, N. Mathews, and S. Mhaisalkar, "Band-gap tuning of lead halide perovskites using a sequential deposition process," *J. Mater. Chem. A* **2**(24), 9221–9225 (2014).
- <sup>140</sup>H. Tan, F. Che, M. Wei, Y. Zhao, M. I. Saidaminov, P. Todorovic, D. Broberg, G. Walters, F. Tan, T. Zhuang, B. Sun, Z. Liang, H. Yuan, E. Fron, J. Kim, Z. Yang, O. Voznyy, M. Asta, and E. H. Sargent, "Dipolar cations confer defect tolerance in wide-bandgap metal halide perovskites," *Nat. Commun.* **9**(1), 3100 (2018).
- <sup>141</sup>M. J. Wu, C. C. Kuo, L. S. Jhuang, P. H. Chen, Y. F. Lai, and F. C. Chen, "Bandgap engineering enhances the performance of mixed-cation perovskite materials for indoor photovoltaic applications," *Adv. Energy Mater.* **9**(37), 1901863 (2019).
- <sup>142</sup>Y. Lin, B. Chen, F. Zhao, X. Zheng, Y. Deng, Y. Shao, Y. Fang, Y. Bai, C. Wang, and J. Huang, "Matching charge extraction contact for wide-bandgap perovskite solar cells," *Adv. Mater.* **29**(26), 1700607 (2017).
- <sup>143</sup>Q. Ye, Y. Zhao, S. Mu, F. Ma, F. Gao, Z. Chu, Z. Yin, P. Gao, X. Zhang, and J. You, "Cesium lead inorganic solar cell with efficiency beyond 18% via reduced charge recombination," *Adv. Mater.* **31**(49), 1905143 (2019).
- <sup>144</sup>X. Hu, X. F. Jiang, X. Xing, L. Nian, X. Liu, R. Huang, K. Wang, H. L. Yip, and G. Zhou, "Wide-bandgap perovskite solar cells with large open-circuit voltage of 1653 mV through interfacial engineering," *Sol. RRL* **2**(8), 1800083 (2018).
- <sup>145</sup>Y.-N. Zhang, B. Li, L. Fu, Y. Zou, Q. Li, and L.-W. Yin, "Enhanced optical absorption and efficient cascade electron extraction based on energy band alignment double absorbers perovskite solar cells," *Sol. Energy Mater. Sol. Cells* **194**, 168–176 (2019).
- <sup>146</sup>M. Chen, M.-G. Ju, A. D. Carl, Y. Zong, R. L. Grimm, J. Gu, X. C. Zeng, Y. Zhou, and N. P. Padture, "Cesium titanium (IV) bromide thin films based stable lead-free perovskite solar cells," *Joule* **2**(3), 558–570 (2018).
- <sup>147</sup>S. Yang, H. Zhao, Y. Han, C. Duan, Z. Liu, and S. Liu, "Europium and acetate Co-doping strategy for developing stable and efficient CsPbI<sub>2</sub>Br perovskite solar cells," *Small* **15**(46), 1904387 (2019).
- <sup>148</sup>H. Zhao, Y. Han, Z. Xu, C. Duan, S. Yang, S. Yuan, Z. Yang, Z. Liu, and S. Liu, "A novel anion doping for stable CsPbI<sub>2</sub>Br perovskite solar cells with an efficiency of 15.56% and an open circuit voltage of 1.30 V," *Adv. Energy Mater.* **9**(40), 1902279 (2019).
- <sup>149</sup>C. Duan, J. Cui, M. Zhang, Y. Han, S. Yang, H. Zhao, H. Bian, J. Yao, K. Zhao, and Z. Liu, "Precursor engineering for ambient-compatible antisolvent-free

- fabrication of high-efficiency  $\text{CsPbI}_2\text{Br}$  perovskite solar cells," *Adv. Energy Mater.* **10**(22), 2000691 (2020).
- <sup>150</sup>H. Bian, D. Bai, Z. Jin, K. Wang, L. Liang, H. Wang, J. Zhang, Q. Wang, and S. F. Liu, "Graded bandgap  $\text{CsPbI}_{2+x}\text{Br}_{1-x}$  perovskite solar cells with a stabilized efficiency of 14.4%," *Joule* **2**(8), 1500–1510 (2018).
- <sup>151</sup>Y. Zhao, A. M. Nardes, and K. Zhu, "Mesoporous perovskite solar cells: Material composition, charge-carrier dynamics, and device characteristics," *Faraday Discuss.* **176**, 301–312 (2014).
- <sup>152</sup>R. Nie, A. Mehta, B. W. Park, H. W. Kwon, J. Im, and S. I. Seok, "Mixed sulfur and iodide-based lead-free perovskite solar cells," *J. Am. Chem. Soc.* **140**(3), 872–875 (2018).
- <sup>153</sup>Q. Xue, G. Chen, M. Liu, J. Xiao, Z. Chen, Z. Hu, X. F. Jiang, B. Zhang, F. Huang, and W. Yang, "Improving film formation and photovoltaic of highly efficient inverted-type perovskite solar cells through the incorporation of new polymeric hole selective layers," *Adv. Energy Mater.* **6**(5), 1502021 (2016).
- <sup>154</sup>W. Zhu, Z. Zhang, W. Chai, Q. Zhang, D. Chen, Z. Lin, J. Chang, J. Zhang, C. Zhang, and Y. Hao, "Band alignment engineering towards high efficiency carbon-based inorganic planar  $\text{CsPbIBr}_2$  perovskite solar cells," *ChemSusChem* **12**(10), 2318–2325 (2019).
- <sup>155</sup>T. Bu, X. Liu, R. Chen, Z. Liu, K. Li, W. Li, Y. Peng, Z. Ku, F. Huang, and Y.-B. Cheng, "Organic/inorganic self-doping controlled crystallization and electronic properties of mixed perovskite solar cells," *J. Mater. Chem. A* **6**(15), 6319–6326 (2018).
- <sup>156</sup>F. Jiang, D. Yang, Y. Jiang, T. Liu, X. Zhao, Y. Ming, B. Luo, F. Qin, J. Fan, and H. Han, "Chlorine-incorporation-induced formation of the layered phase for antimony-based lead-free perovskite solar cells," *J. Am. Chem. Soc.* **140**(3), 1019–1027 (2018).
- <sup>157</sup>B. W. Park, B. Philippe, X. Zhang, H. Rensmo, G. Boschloo, and E. M. Johansson, "Bismuth based hybrid perovskites  $\text{A}_3\text{Bi}_2\text{I}_9$  ( $\text{A}$ : Methylammonium or cesium) for solar cell application," *Adv. Mater.* **27**(43), 6806–6813 (2015).
- <sup>158</sup>F. Umar, J. Zhang, Z. Jin, I. Muhammad, X. Yang, H. Deng, K. Jahangeer, Q. Hu, H. Song, and J. Tang, "Dimensionality controlling of  $\text{Cs}_3\text{Sb}_2\text{I}_9$  for efficient all-inorganic planar thin film solar cells by HCl-assisted solution method," *Adv. Opt. Mater.* **7**(5), 1801368 (2019).
- <sup>159</sup>Y. Zhang, Y. Liang, Y. Wang, F. Guo, L. Sun, and D. Xu, "Planar FAPbBr<sub>3</sub> solar cells with power conversion efficiency above 10%," *ACS Energy Lett.* **3**(8), 1808–1814 (2018).
- <sup>160</sup>J. Duan, Y. Zhao, B. He, and Q. Tang, "High-purity inorganic perovskite films for solar cells with 9.72% efficiency," *Angew. Chem. Int. Ed.* **130**(14), 3849–3853 (2018).
- <sup>161</sup>G. Liao, J. Duan, Y. Zhao, and Q. Tang, "Toward fast charge extraction in all-inorganic  $\text{CsPbBr}_3$  perovskite solar cells by setting intermediate energy levels," *Sol. Energy* **171**, 279–285 (2018).
- <sup>162</sup>X. Wan, Z. Yu, W. Tian, F. Huang, S. Jin, X. Yang, Y.-B. Cheng, A. Hagfeldt, and L. Sun, "Efficient and stable planar all-inorganic perovskite solar cells based on high-quality  $\text{CsPbBr}_3$  films with controllable morphology," *J. Energy Chem.* **46**, 8–15 (2020).
- <sup>163</sup>J. Zhu, M. Tang, B. He, W. Zhang, X. Li, Z. Gong, H. Chen, Y. Duan, and Q. Tang, "Improved charge extraction through interface engineering for 10.12% efficiency and stable  $\text{CsPbBr}_3$  perovskite solar cells," *J. Mater. Chem. A* **8**(40), 20987–20997 (2020).
- <sup>164</sup>Y. Zhao, J. Duan, Y. Wang, X. Yang, and Q. Tang, "Precise stress control of inorganic perovskite films for carbon-based solar cells with an ultrahigh voltage of 1.622 V," *Nano Energy* **67**, 104286 (2020).
- <sup>165</sup>Y. Zhao, J. Duan, H. Yuan, Y. Wang, X. Yang, B. He, and Q. Tang, "Using  $\text{SnO}_2$  QDs and  $\text{CsMBr}_3$  ( $\text{M} = \text{Sn}, \text{Bi}, \text{Cu}$ ) QDs as charge-transporting materials for 10.6%-efficiency all-inorganic  $\text{CsPbBr}_3$  perovskite solar cells with an ultrahigh open-circuit voltage of 1.610 V," *Sol. RRL* **3**(3), 1800284 (2019).
- <sup>166</sup>C. H. Ng, T. S. Ripolles, K. Hamada, S. H. Teo, H. N. Lim, J. Bisquert, and S. Hayase, "Tunable open circuit voltage by engineering inorganic cesium lead bromide/iodide perovskite solar cells," *Sci. Rep.* **8**(1), 2482 (2018).
- <sup>167</sup>M. Safdari, P. H. Svensson, M. T. Hoang, I. Oh, L. Kloof, and J. M. Gardner, "Layered 2D alkyldiammonium lead iodide perovskites: Synthesis, characterization, and use in solar cells," *J. Mater. Chem. A* **4**(40), 15638–15646 (2016).
- <sup>168</sup>Y. Zhao, H. Xu, Y. Wang, X. Yang, J. Duan, and Q. Tang, "10.34%-efficient integrated  $\text{CsPbBr}_3$ /bulk-heterojunction solar cells," *J. Power Sources* **440**, 227151 (2019).
- <sup>169</sup>G. Murugadoss, R. Thangamuthu, S. M. S. Kumar, N. Anandhan, M. R. Kumar, and A. Rathishkumar, "Synthesis of ligand-free, large scale with high quality all-inorganic  $\text{CsPbI}_3$  and  $\text{CsPb}_2\text{Br}_5$  nanocrystals and fabrication of all-inorganic perovskite solar cells," *J. Alloys Compd.* **787**, 17–26 (2019).
- <sup>170</sup>L. Zuo, X. Shi, W. Fu, and A. K. Y. Jen, "Highly efficient semitransparent solar cells with selective absorption and tandem architecture," *Adv. Mater.* **31**(36), 1901683 (2019).
- <sup>171</sup>E. Greul, M. L. Petrus, A. Binek, P. Docampo, and T. Bein, "Highly stable, phase pure  $\text{Cs}_2\text{AgBiBr}_6$  double perovskite thin films for optoelectronic applications," *J. Mater. Chem. A* **5**(37), 19972–19981 (2017).
- <sup>172</sup>T. Bu, J. Li, H. Li, C. Tian, J. Su, G. Tong, L. K. Ono, C. Wang, Z. Lin, and N. J. S. Chai, "Lead halide-templated crystallization of methylamine-free perovskite for efficient photovoltaic modules," *Science* **372**(6548), 1327–1332 (2021).